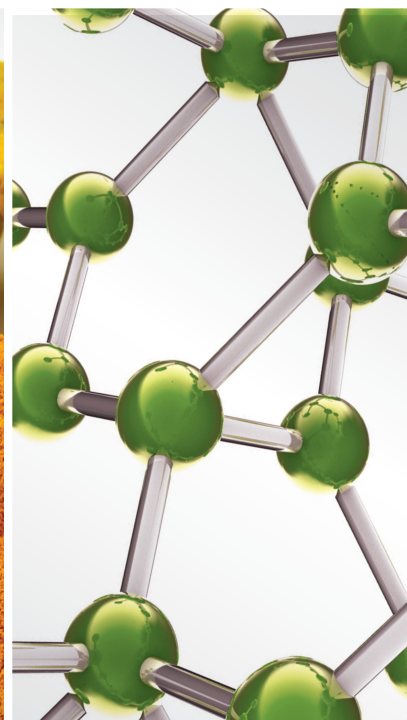
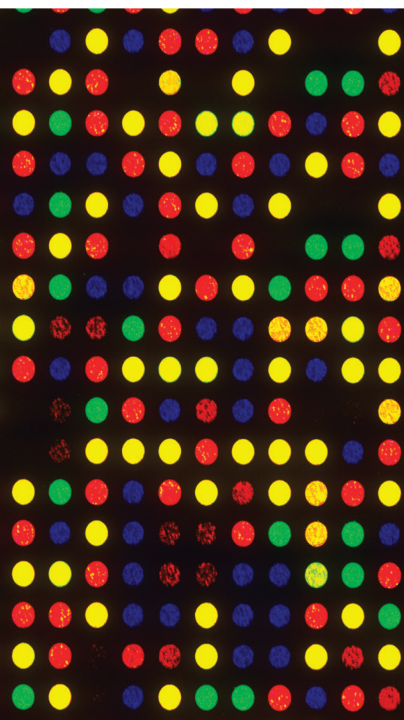


Nanodelivery for Efficient Natural Product-based Nanomedicine

Lead Guest Editor: Fernanda Maria Policarpo Tonelli

Guest Editors: H.C. Ananda Murthy and José Rafael de Almeida





Nanodelivery for Efficient Natural Product-based Nanomedicine

**Nanodelivery for Efficient Natural
Product-based Nanomedicine**

Lead Guest Editor: Fernanda Maria Policarpo
Tonelli

Guest Editors: H.C. Ananda Murthy and José
Rafael de Almeida



Copyright © 2023 Hindawi Limited. All rights reserved.

This is a special issue published in "Evidence-Based Complementary and Alternative Medicine." All articles are open access articles distributed under the Creative Commons Attribution License, which permits unrestricted use, distribution, and reproduction in any medium, provided the original work is properly cited.

Chief Editor

Jian-Li Gao , China








Associate Editors

Hyunsu Bae , Republic of Korea
Raffaele Capasso , Italy
Jae Youl Cho , Republic of Korea
Caigan Du , Canada
Yuewen Gong , Canada
Hai-dong Guo , China
Kuzhuvelil B. Harikumar , India
Ching-Liang Hsieh , Taiwan
Cheorl-Ho Kim , Republic of Korea
Victor Kuete , Cameroon
Hajime Nakae , Japan
Yoshiji Ohta , Japan
Olumayokun A. Olajide , United Kingdom
Chang G. Son , Republic of Korea
Shan-Yu Su , Taiwan
Michał Tomczyk , Poland
Jenny M. Wilkinson , Australia

Academic Editors

Eman A. Mahmoud , Egypt
Ammar AL-Farga , Saudi Arabia
Smail Aazza , Morocco
Nahla S. Abdel-Azim, Egypt
Ana Lúcia Abreu-Silva , Brazil
Gustavo J. Acevedo-Hernández , Mexico
Mohd Adnan , Saudi Arabia
Jose C Adsuar , Spain
Sayeed Ahmad, India
Touqeer Ahmed , Pakistan
Basiru Ajiboye , Nigeria
Bushra Akhtar , Pakistan
Fahmida Alam , Malaysia
Mohammad Jahoor Alam, Saudi Arabia
Clara Albani, Argentina
Ulysses Paulino Albuquerque , Brazil
Mohammed S. Ali-Shtayeh , Palestinian Authority
Ekram Alias, Malaysia
Terje Alraek , Norway
Adolfo Andrade-Cetto , Mexico
Letizia Angiolella , Italy
Makoto Arai , Japan

Daniel Dias Rufino Arcanjo , Brazil
Duygu AĞAGÜNDÜZ , Turkey
Neda Baghban , Iran
Samra Bashir , Pakistan
Rusliza Basir , Malaysia
Jairo Kenupp Bastos , Brazil
Arpita Basu , USA
Mateus R. Beguelini , Brazil
Juana Benedí, Spain
Samira Boulbaroud, Morocco
Mohammed Bourhia , Morocco
Abdelhakim Bouyahya, Morocco
Nunzio Antonio Cacciola , Italy
Francesco Cardini , Italy
María C. Carpinella , Argentina
Harish Chandra , India
Guang Chen, China
Jianping Chen , China
Kevin Chen, USA
Mei-Chih Chen, Taiwan
Xiaojia Chen , Macau
Evan P. Cherniack , USA
Giuseppina Chianese , Italy
Kok-Yong Chin , Malaysia
Lin China, China
Salvatore Chirumbolo , Italy
Hwi-Young Cho , Republic of Korea
Jeong June Choi , Republic of Korea
Jun-Yong Choi, Republic of Korea
Kathrine Bisgaard Christensen , Denmark
Shuang-En Chuang, Taiwan
Ying-Chien Chung , Taiwan
Francisco José Cidral-Filho, Brazil
Daniel Collado-Mateo , Spain
Lisa A. Conboy , USA
Kieran Cooley , Canada
Edwin L. Cooper , USA
José Otávio do Amaral Corrêa , Brazil
Maria T. Cruz , Portugal
Huantian Cui , China
Giuseppe D'Antona , Italy
Ademar A. Da Silva Filho , Brazil
Chongshan Dai, China
Laura De Martino , Italy
Josué De Moraes , Brazil

Arthur De Sá Ferreira , Brazil
Nunziatina De Tommasi , Italy
Marinella De leo , Italy
Gourav Dey , India
Dinesh Dhamecha, USA
Claudia Di Giacomo , Italy
Antonella Di Sotto , Italy
Mario Dioguardi, Italy
Jeng-Ren Duann , USA
Thomas Effërth , Germany
Abir El-Alfy, USA
Mohamed Ahmed El-Esawi , Egypt
Mohd Ramli Elvy Suhana, Malaysia
Talha Bin Emran, Japan
Roger Engel , Australia
Karim Ennouri , Tunisia
Giuseppe Esposito , Italy
Tahereh Eteraf-Oskouei, Iran
Robson Xavier Faria , Brazil
Mohammad Fattahi , Iran
Keturah R. Faurot , USA
Piergiorgio Fedeli , Italy
Laura Ferraro , Italy
Antonella Fioravanti , Italy
Carmen Formisano , Italy
Hua-Lin Fu , China
Liz G Müller , Brazil
Gabino Garrido , Chile
Safoora Gharibzadeh, Iran
Muhammad N. Ghayur , USA
Angelica Gomes , Brazil
Elena González-Burgos, Spain
Susana Gorzalczany , Argentina
Jiangyong Gu , China
Maruti Ram Gudavalli , USA
Jian-You Guo , China
Shanshan Guo, China
Narcís Gusi , Spain
Svein Haavik, Norway
Fernando Hallwass, Brazil
Gajin Han , Republic of Korea
Ihsan Ul Haq, Pakistan
Hicham Harhar , Morocco
Mohammad Hashem Hashempur , Iran
Muhammad Ali Hashmi , Pakistan

Waseem Hassan , Pakistan
Sandrina A. Heleno , Portugal
Pablo Herrero , Spain
Soon S. Hong , Republic of Korea
Md. Akil Hossain , Republic of Korea
Muhammad Jahangir Hossen , Bangladesh
Shih-Min Hsia , Taiwan
Changmin Hu , China
Tao Hu , China
Weicheng Hu , China
Wen-Long Hu, Taiwan
Xiao-Yang (Mio) Hu, United Kingdom
Sheng-Teng Huang , Taiwan
Ciara Hughes , Ireland
Attila Hunyadi , Hungary
Liaqat Hussain , Pakistan
Maria-Carmen Iglesias-Osma , Spain
Amjad Iqbal , Pakistan
Chie Ishikawa , Japan
Angelo A. Izzo, Italy
Satveer Jagwani , USA
Rana Jamous , Palestinian Authority
Muhammad Saeed Jan , Pakistan
G. K. Jayaprakasha, USA
Kyu Shik Jeong, Republic of Korea
Leopold Jirovetz , Austria
Jeeyoun Jung , Republic of Korea
Nurkhalida Kamal , Saint Vincent and the
Grenadines
Atsushi Kameyama , Japan
Kyungsu Kang, Republic of Korea
Wenyi Kang , China
Shao-Hsuan Kao , Taiwan
Nasiara Karim , Pakistan
Morimasa Kato , Japan
Kumar Katragunta , USA
Deborah A. Kennedy , Canada
Washim Khan, USA
Bonglee Kim , Republic of Korea
Dong Hyun Kim , Republic of Korea
Junghyun Kim , Republic of Korea
Kyungho Kim, Republic of Korea
Yun Jin Kim , Malaysia
Yoshiyuki Kimura , Japan

Nebojša Kladar , Serbia
Mi Mi Ko , Republic of Korea
Toshiaki Kogure , Japan
Malcolm Koo , Taiwan
Yu-Hsiang Kuan , Taiwan
Robert Kubina , Poland
Chan-Yen Kuo , Taiwan
Kuang C. Lai , Taiwan
King Hei Stanley Lam, Hong Kong
Faniel Lampiao, Malawi
Ilaria Lampronti , Italy
Mario Ledda , Italy
Harry Lee , China
Jeong-Sang Lee , Republic of Korea
Ju Ah Lee , Republic of Korea
Kyu Pil Lee , Republic of Korea
Namhun Lee , Republic of Korea
Sang Yeoup Lee , Republic of Korea
Ankita Leekha , USA
Christian Lehmann , Canada
George B. Lenon , Australia
Marco Leonti, Italy
Hua Li , China
Min Li , China
Xing Li , China
Xuqi Li , China
Yi-Rong Li , Taiwan
Vuanghao Lim , Malaysia
Bi-Fong Lin, Taiwan
Ho Lin , Taiwan
Shuibin Lin, China
Kuo-Tong Liou , Taiwan
I-Min Liu, Taiwan
Suhuan Liu , China
Xiaosong Liu , Australia
Yujun Liu , China
Emilio Lizarraga , Argentina
Monica Loizzo , Italy
Nguyen Phuoc Long, Republic of Korea
Zaira López, Mexico
Chunhua Lu , China
Ângelo Luís , Portugal
Anderson Luiz-Ferreira , Brazil
Ivan Luzardo Luzardo-Ocampo, Mexico

Michel Mansur Machado , Brazil
Filippo Maggi , Italy
Juraj Majtan , Slovakia
Toshiaki Makino , Japan
Nicola Malafronte, Italy
Giuseppe Malfa , Italy
Francesca Mancianti , Italy
Carmen Mannucci , Italy
Juan M. Manzanque , Spain
Fatima Martel , Portugal
Carlos H. G. Martins , Brazil
Maulidiani Maulidiani, Malaysia
Andrea Maxia , Italy
Avijit Mazumder , India
Isac Medeiros , Brazil
Ahmed Mediani , Malaysia
Lewis Mehl-Madrona, USA
Ayikoé Guy Mensah-Nyagan , France
Oliver Micke , Germany
Maria G. Miguel , Portugal
Luigi Milella , Italy
Roberto Miniero , Italy
Letteria Minutoli, Italy
Prashant Modi , India
Daniel Kam-Wah Mok, Hong Kong
Changjong Moon , Republic of Korea
Albert Moraska, USA
Mark Moss , United Kingdom
Yoshiharu Motoo , Japan
Yoshiki Mukudai , Japan
Sakthivel Muniyan , USA
Saima Muzammil , Pakistan
Benoit Banga N'guessan , Ghana
Massimo Nabissi , Italy
Siddavaram Nagini, India
Takao Namiki , Japan
Srinivas Nammi , Australia
Krishnadas Nandakumar , India
Vitaly Napadow , USA
Edoardo Napoli , Italy
Jorddy Neves Cruz , Brazil
Marcello Nicoletti , Italy
Eliud Nyaga Mwaniki Njagi , Kenya
Cristina Nogueira , Brazil

Sakineh Kazemi Noureini , Iran
Rômulo Dias Novaes, Brazil
Martin Offenbaecher , Germany
Oluwafemi Adeleke Ojo , Nigeria
Olufunmiso Olusola Olajuyigbe , Nigeria
Luís Flávio Oliveira, Brazil
Mozaniel Oliveira , Brazil
Atolani Olubunmi , Nigeria
Abimbola Peter Oluyori , Nigeria
Timothy Omara, Austria
Chiagoziem Anariochi Otuechere , Nigeria
Sokcheon Pak , Australia
Antônio Palumbo Jr, Brazil
Zongfu Pan , China
Siyaram Pandey , Canada
Niranjan Parajuli , Nepal
Gunhyuk Park , Republic of Korea
Wansu Park , Republic of Korea
Rodolfo Parreira , Brazil
Mohammad Mahdi Parvizi , Iran
Luiz Felipe Passero , Brazil
Mitesh Patel, India
Claudia Helena Pellizzon , Brazil
Cheng Peng, Australia
Weijun Peng , China
Sonia Piacente, Italy
Andrea Pieroni , Italy
Haifa Qiao , USA
Cláudia Quintino Rocha , Brazil
DANIELA RUSSO , Italy
Muralidharan Arumugam Ramachandran,
Singapore
Manzoor Rather , India
Miguel Rebollo-Hernanz , Spain
Gauhar Rehman, Pakistan
Daniela Rigano , Italy
José L. Rios, Spain
Francisca Rius Diaz, Spain
Eliana Rodrigues , Brazil
Maan Bahadur Rokaya , Czech Republic
Mariangela Rondanelli , Italy
Antonietta Rossi , Italy
Mi Heon Ryu , Republic of Korea
Bashar Saad , Palestinian Authority
Sabi Saheed, South Africa






Mohamed Z.M. Salem , Egypt
Avni Sali, Australia
Andreas Sandner-Kiesling, Austria
Manel Santafe , Spain
José Roberto Santin , Brazil
Tadaaki Satou , Japan
Roland Schoop, Switzerland
Sindy Seara-Paz, Spain
Veronique Seidel , United Kingdom
Vijayakumar Sekar , China
Terry Selfe , USA
Arham Shabbir , Pakistan
Suzana Shahar, Malaysia
Wen-Bin Shang , China
Xiaofei Shang , China
Ali Sharif , Pakistan
Karen J. Sherman , USA
San-Jun Shi , China
Insop Shim , Republic of Korea
Maria Im Hee Shin, China
Yukihiro Shoyama, Japan
Morry Silberstein , Australia
Samuel Martins Silvestre , Portugal
Preet Amol Singh, India
Rajeev K Singla , China
Kuttulebbai N. S. Sirajudeen , Malaysia
Slim Smaoui , Tunisia
Eun Jung Sohn , Republic of Korea
Maxim A. Solovchuk , Taiwan
Young-Jin Son , Republic of Korea
Chengwu Song , China
Vanessa Steenkamp , South Africa
Annarita Stringaro , Italy
Keiichiro Sugimoto , Japan
Valeria Sulsen , Argentina
Zewei Sun , China
Sharifah S. Syed Alwi , United Kingdom
Orazio Tagliatalata-Scafati , Italy
Takashi Takeda , Japan
Gianluca Tamagno , Ireland
Hongxun Tao, China
Jun-Yan Tao , China
Lay Kek Teh , Malaysia
Norman Temple , Canada

Kamani H. Tennekoon , Sri Lanka
Seong Lin Teoh, Malaysia
Menaka Thounaojam , USA
Jinhui Tian, China
Zipora Tietel, Israel
Loren Toussaint , USA
Riaz Ullah , Saudi Arabia
Philip F. Uzor , Nigeria
Luca Vanella , Italy
Antonio Vassallo , Italy
Cristian Vergallo, Italy
Miguel Vilas-Boas , Portugal
Aristo Vojdani , USA
Yun WANG , China
QIBIAO WU , Macau
Abraham Wall-Medrano , Mexico
Chong-Zhi Wang , USA
Guang-Jun Wang , China
Jinan Wang , China
Qi-Rui Wang , China
Ru-Feng Wang , China
Shu-Ming Wang , USA
Ting-Yu Wang , China
Xue-Rui Wang , China
Youhua Wang , China
Kenji Watanabe , Japan
Jintanaporn Wattanathorn , Thailand
Silvia Wein , Germany
Katarzyna Winska , Poland
Sok Kuan Wong , Malaysia
Christopher Worsnop, Australia
Jih-Huah Wu , Taiwan
Sijin Wu , China
Xian Wu, USA
Zuoqi Xiao , China
Rafael M. Ximenes , Brazil
Guoqiang Xing , USA
JiaTuo Xu , China
Mei Xue , China
Yong-Bo Xue , China
Haruki Yamada , Japan
Nobuo Yamaguchi, Japan
Junqing Yang, China
Longfei Yang , China

Mingxiao Yang , Hong Kong
Qin Yang , China
Wei-Hsiung Yang, USA
Swee Keong Yeap , Malaysia
Albert S. Yeung , USA
Ebrahim M. Yimer , Ethiopia
Yoke Keong Yong , Malaysia
Fadia S. Youssef , Egypt
Zhilong Yu, Canada
RONGJIE ZHAO , China
Sultan Zahiruddin , USA
Armando Zarrelli , Italy
Xiaobin Zeng , China
Y Zeng , China
Fangbo Zhang , China
Jianliang Zhang , China
Jiu-Liang Zhang , China
Mingbo Zhang , China
Jing Zhao , China
Zhangfeng Zhong , Macau
Guoqi Zhu , China
Yan Zhu , USA
Suzanna M. Zick , USA
Stephane Zingue , Cameroon



Contents

Novel Benzothiazole Derivatives Synthesis and its Analysis as Diuretic Agents

Durgaprasad Kemisetti, Ruhul Amin , Faruk Alam , Amel Gacem, Talha Bin Emran , Taghreed Alsufyani, Mohammed S. Alqahtani , Saiful Islam , Mohammed Mahbubul Matin, and Mohammed Jameel


Research Article (12 pages), Article ID 5460563, Volume 2023 (2023)

The Effect of Cytotoxicity and Antimicrobial of Synthesized CuO NPs from Propolis on HEK-293 Cells and *Lactobacillus acidophilus*

Yasamin Seyyed Hajizadeh, Ebrahim Babapour, Naser Harzandi, Mohsen Yazdanian , and Reza Ranjbar 


Research Article (11 pages), Article ID 1430839, Volume 2023 (2023)

The Feasibility of Choosing D4 Embryo Transfer—Analysis of Nanomaterials Affecting the Outcome of Frozen-Thaw Embryo Transfer

Chang Tan, Xiliang Wang, Lishuang Luo, Jinyan Zhang, Pengshu Zou, Wei Wei, and Yuexin Yu 

Research Article (7 pages), Article ID 1364865, Volume 2022 (2022)






Identification of CeRNA Regulatory Networks in Atrial Fibrillation Using Nanodelivery

Ping Lin, Lingqiang Meng, and Lei Lyu 

Research Article (9 pages), Article ID 1046905, Volume 2022 (2022)

Research Article

Novel Benzothiazole Derivatives Synthesis and its Analysis as Diuretic Agents

Durgaprasad Kemiseti,¹ Ruhul Amin ,¹ Faruk Alam ,¹ Amel Gacem,² Talha Bin Emran ,^{3,4} Taghreed Alsufyani,⁵ Mohammed S. Alqahtani ,^{6,7,8} Saiful Islam ,⁹ Mohammed Mahbubul Matin,¹⁰ and Mohammed Jameel¹¹

¹Faculty of Pharmaceutical Science, Assam Down Town University, Panikhaiti, Guwahati, Assam, India

²Department of Physics, Faculty of Sciences, University 20 Août 1955, Skikda, Algeria

³Department of Pharmacy, BGC Trust University Bangladesh, Chittagong 4381, Bangladesh

⁴Department of Pharmacy, Faculty of Allied Health Sciences, Daffodil International University, Dhaka 1207, Bangladesh

⁵Department of Chemistry, College of Science, Taif University, P.O. Box 11099, Taif 21944, Saudi Arabia

⁶Radiological Sciences Department, College of Applied Medical Sciences, King Khalid University, Abha 61421, Saudi Arabia

⁷BioImaging Unit, Space Research Centre, Michael Atiyah Building, University of Leicester, Leicester, LE1 7RH, UK

⁸Research Center for Advanced Materials Science (RCAMS), King Khalid University, Postcode: 9004, Zip Code: 61413, Abha, Saudi Arabia

⁹Civil Engineering Department, College of Engineering, King Khalid University, Abha 61421, Saudi Arabia

¹⁰Bioorganic and Medicinal Chemistry Laboratory, Faculty of Science, Department of Chemistry, University of Chittagong, Chittagong 4331, Bangladesh

¹¹Department of Civil Engineering, College of Engineering, King Khalid University, Abha, Saudi Arabia

Correspondence should be addressed to Ruhul Amin; ruhulgp18@gmail.com and Talha Bin Emran; talhabmb@bgctub.ac.bd

Received 22 August 2022; Revised 18 September 2022; Accepted 22 September 2022; Published 12 April 2023

Academic Editor: Fernanda Tonelli

Copyright © 2023 Durgaprasad Kemiseti et al. This is an open access article distributed under the Creative Commons Attribution License, which permits unrestricted use, distribution, and reproduction in any medium, provided the original work is properly cited.

Benzothiazoles, an anticonvulsant, antiviral, antihypertensive, and cancer-fighting medication of the heterocyclic scaffold family, also acts as antibacterial and antiviral agents. There is much interest in this chemical's production because of the strong and vital biological action it possesses. Substituted aromatic aldehydes were combined with 2-amino-benzothiazole-6-sulfonic acid amides, or Schiff base derivatives, to create Schiff base derivatives. Recrystallized, characterized, and tested for diuretic efficacy in vivo using online tools, m.p. (melting point), Rf, FTIR (Fourier transform infrared), ¹H-NMR (proton nuclear magnetic resonance) data. The molecular characteristics of all the substances created were estimated using Lipinski's rule of 5, OSIRIS (software molecular property explorer, Molsoft, and Autodock 4.0 docking software). Male Wistar rats were used to make all the compounds traditionally in order to test for diuretic activity. Neither the elemental nor the spectral information for the synthesized compounds disagreed. There were five different methods used to evaluate these compounds: Lipinski rule of five, Molsoft to determine molecular characteristics, PASS (prediction of activity spectra for substances) values to determine the diuretic effect, and OSIRIS software to determine toxicology. In order to investigate the diuretic effects of the selected drugs, docking analysis was used. Acetazolamide was shown to have a diuretic effect that was superior to that of compounds **IIIb** and **IIIe**, whereas 2-[(E)-[(3-hydroxyphenyl)methylidene]amino]-1,3-benzothiazole-6-sulfonamide (**IIIb**) was found to be the most promising potential.

1. Introduction

Patients with life-threatening diseases such as congestive heart failure, renal disease, hypertension, acute oedema of

the lungs, and ascites may all improve from drug-induced diuresis. Because diuretics all cause potassium loss even if they work well at boosting sodium excretion, researchers have been searching for new diuretic medications that do not

cause potassium loss yet still work well at maintaining therapeutic efficacy [1, 2].

Derivatives of 2-aminobenzothiazoles are reported to have diverse biological activities like cytotoxicity, anti-inflammatory, analgesic, anthelmintic, antiviral, antidiabetic, antimicrobial, antileishmanial, anticonvulsant, Alzheimer's disease, and calcium channel blocking [3–6]. The present study was carried out on 6-sulfonamide containing 2-aminobenzothiazole Schiff bases derivatives as lead molecules of the study with the aid of docking for evaluating their diuretic activity, which is an adjunct therapy in treating hypertension [7–9].

It is a common practice in SBDD to use molecular docking because it can accurately anticipate the shape of small-molecule ligands in the target-binding site. In addition, it is one of the most reliable approaches. Molecular docking has been an essential method in drug discovery since the first algorithms were developed in the 1980s [10]. In order to find the most likely binding configurations, two processes must be completed: A wide range of probable binding modes is examined, and the interaction energy associated with each of these binding conformations is accurately predicted [11].

The software used to determine if a molecule is a drug or not follows the Lipinski rule of five [12]. It includes information on molecular weight, hydrogen bond donor, hydrogen bond acceptor, logP value, and molar refractivity. Molsoft L.L.C drug likeness and molecular property prediction provides a molecule's molecular formula, molecular weight, hydrogen bond acceptor, hydrogen bond donor, MolLogP, MolLogS, MolPSA, MolVol, pKa, BBB score, number of stereo centres, and drug likeness score [13–15]. OSIRIS property explorer offers information if a molecule [16], if produced, creates any toxicity impact by exhibiting in the window on the screen; green colour indicates nontoxic while red colour harmful. Other data like solubility, TPSA, clogP, drug likeness, and drug score are also provided. The online freeware PASS (prediction of activity spectra for substances) determines whether a chemical is physiologically active as *Pa* or inert as *Pi*. Molinspiration and SWISS ADME [17] software's were used to determine drug activity ADME, physicochemical characteristics, GI absorption, drug likeness, GPCR ligand, ion channel modulator, kinase inhibitor, nuclear receptor ligand, protease inhibitor and enzyme inhibitor, and bioavailability score. Based on the premise, benzthiazoles (Figure 1) have diuretic action as such, the experiment was planned to synthesize derivatives if they exhibit diuretic activity.

2. Materials and Methods

There were three types of beakers used in this experiment: dry Borosil glass, round bottomed glass, and conical glass. MERCK precoated silica gel plates were utilized for TLC monitoring, and a JASCO UV chamber was employed to see spots in TLC.

Instruments for visual melting range measurements were purchased from Lab India. KBr (potassium bromide) disc on FTIR 8300, and KBr press Shimadzu were used to

record the IR spectra of compound **IIIb**. The ¹H-NMR spectra of the synthesized chemical **IIIb** were acquired on a BRUKER-400 MHz spectrometer using DMSO as the solvent, and the results were analyzed. Digital flame photometer Cisco 381 was used for the estimation of ions.

2.1. Chemistry. The synthetic procedures that were followed in order to get the target compounds **IIIa-i** were represented in diagrams. The structures of synthesized substances were determined on the basis of elemental analysis and spectrum data collected throughout the process. The preceding starting ingredients for the synthesis of 2-amino-benzothiazole-6-sulfonic acid amide (**II**), which is a cyclisation process, were para-amino sulphanilamide and ammonium thiocyanate. Compounds **IIIa-i** were first made by reacting equimolar quantities of (**II**) with suitable aldehydes in 100% alcohol, which is an imine production reaction followed by a nucleophilic addition reaction. Compounds **IIIb-i** were then synthesized in the same manner [18].

2.1.1. General Method for the Synthesis of 2-amino-benzothiazole-6-sulfonic acid amide (II). Everything was combined with glacial acetic acid, which had been precooled to 5°C, and 0.06 mol of sodium hydroxide and 0.06 mol of *p*-aminosulphanilamide. This mixture was kept in an ice bath and mechanically agitated while bromine (0.02 mol) was slowly introduced from an infusion funnel, maintaining a temperature rise of no more than 4–5°C during the process. The results were stunning. For an additional three hours, the mixture was continually churned in an ice bath at a temperature ranging from 0 to 10 °C. Acid was used to remove the hydrochloride salt from the filter and dry it before dissolving it in hot water. The water was used to wash the solution after it had been neutralized with aq. NH₃ solution (25 percent) and filtered. The needed pure chemical was obtained using benzene recrystallization (**II**) [18–20].

Yellowish brown; m.p. 230°C; Yield 80%.

2.1.2. General Method for the Synthesis of Schiff's Bases of 2-amino benzothiazole Compounds (IIIa-g). In 20 mL of ethanol, 6-nitro-2-aminobenzothiazole **2a** (0.025 mol) was dissolved and 10 mL of ethanol was added in drops to the substituted aromatic aldehyde (0.030 mol). Twenty-four hours at room temperature were spent stirring the reaction mixture. A mixture of ethyl acetate:chloroform (1 : 2) was then evaporated, and the result was recrystallized from this combination to yield (**IIIa-g**) [21, 22].

2.2. In Silico Tools. Softwares of Lipinski rule of Five, Molsoft, PASS Online, OSIRIS Property Explorer, were used online [23–25].

AutoDock is a programme for simulating molecular models. Protein ligand docking is a particular strength of this method. Vina is an upgraded version of Auto Dock 4.0 and Auto Dock 4.2. Using Auto Dock 4.0, researchers follow four basic phases in the process, including synthesis of proteins, ligands, and grids [11].

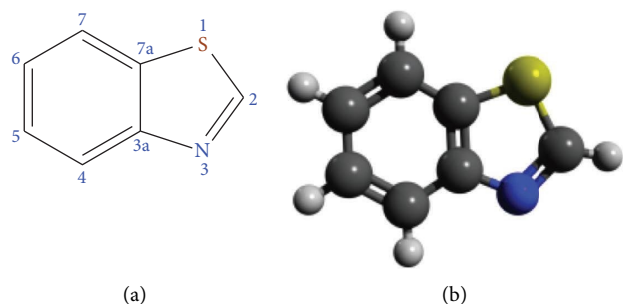


FIGURE 1: Benzothiazole. (a) Structure. (b) Model (ball and stick).

2.3. Molecular Docking Studies. Studies of enzyme-ligand interactions *in vivo* may be predicted by molecular docking studies. In order to do molecular docking experiments on the 3D structure of CA-II enzyme, we used 64-bit operating system under Windows 10 with an HP computer [Intel core i5 8th generation processor, 12 gigabytes of ram]. The 3D structure of the enzyme CA-II was downloaded from the RCSB-Protein Data Bank (PDB ID: 3BL1).

The enzyme's structure was improved and verified for any missing atoms, bonds, or connections. Remaining residues were carefully removed, omitting ligands and water molecules. Building the ligand molecules required the use of the builder molecule, which reduced their energy. It created an active site by using grid box tools, and an energy-efficient conformer was selected and its energy was minimized. For 3BL1 compounds, **IIIb**, **IIIe**, and standard, the optimum binding modes are shown as illustrated in Figures 2–4.

2.4. Effect on Electrolyte Concentration. Flame photometry was used to measure the concentration of Na⁺ and K⁺ ions. For flame photometric examination, the major standard solutions of sodium and potassium were produced at a weight concentration of 1000 ppm each.

This method was used to dilute these solutions to the correct concentrations before usage. Distilled water was used

to dilute the urine (1–3 ml) to a final volume of 100 ml, and the resulting diluted solution was used to measure the ions Na⁺ and K⁺ in the urine.

2.5. Evaluation of Diuretic Activity. Methods of diuretic activity were carried out utilizing Lipschitz's approach. Institutional Animal Ethics Committee 4/IAEC/VCOP/2019 Central Animal House, Vaagdevi College of Pharmacy, Hanamkonda, Warangal approved the study's experimental procedure.

An acute investigation of diuretic action was conducted on five groups of male Wister rats ($n=6$) whose weight was about 100–120 g that had been acclimatized for 10 days. Each group is housed in a metabolic cage with a wire mesh bottom and a urine collection funnel. The faeces are caught in stainless steel sieves in the funnel, which enable the urine to go through. A regular diet of Altromin pellets and water were given to the rats. The rats were fed and watered for fifteen hours before the experiment in order to measure diuretic activity. Gently compressing the pelvic region and tugging the tails of the animals helped empty their bladders. Individual cages for each animal were put 24 hours prior to the experiment's start date for environmental adaption. 0.9 percent NaCl solution was used to provide a dosage of 25 and 45 mg/kg of body weight, respectively. Only 0.9 percent NaCl solution is given to the control group. Both 25 and 45 mg/kg body weight of the test compounds were compared to the conventional diuretic acetazolamide in a 0.9 percent NaCl solution (Scheme 1).

A graduated cylinder was used to collect urine, and the volume was recorded every five hours and every 24 hours. Fluorescence photometric analysis was used to determine sodium and potassium concentrations, which were represented as mmol/L [26].

The amount of diuretic activity was determined by using the following formula:

$$\text{Urinary Excretion} = \frac{\text{Total urinary output (Vo)}}{\text{Total liquid administered (Vt)}} \times 100, \quad (1)$$

$$\text{Diuretic Action} = \frac{\text{Urinary Excretion in test group (UEt)}}{\text{Urinary Excretion in control group (UEc)}}, \quad (2)$$

$$\text{Diuretic Action} = \frac{\text{Diuretic action of the test group (DAT)}}{\text{Diuretic action of urea group (DAu)}}, \quad (3)$$

$$\text{Lipschitz value} = \frac{\text{Urinary Excretion of test group (UEt)}}{\text{Urinary Excretion of urea group (UEu)}}. \quad (4)$$

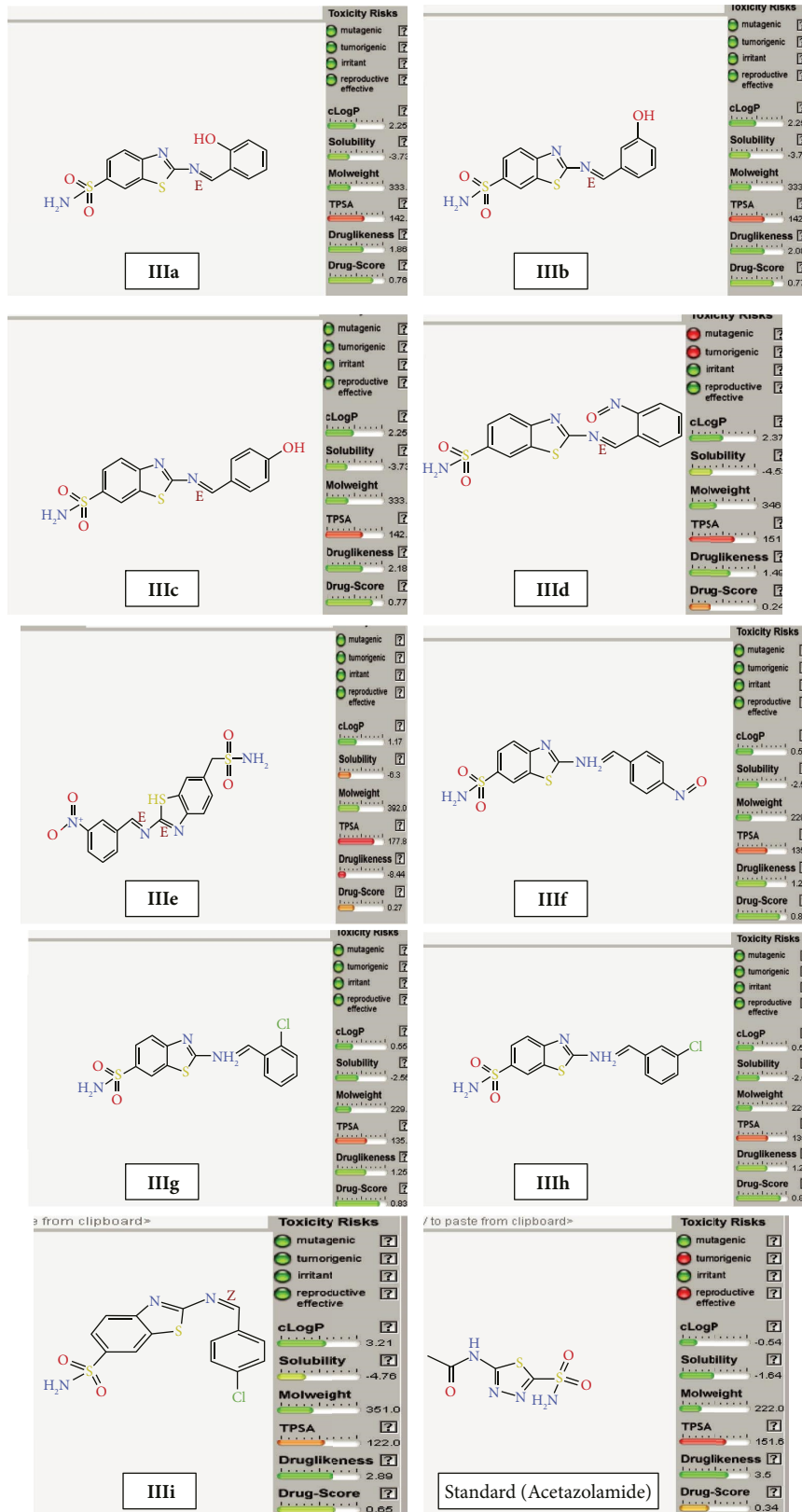


FIGURE 2: Molecular property explorers OSIRIS and standard for compounds IIIa-IIIi.

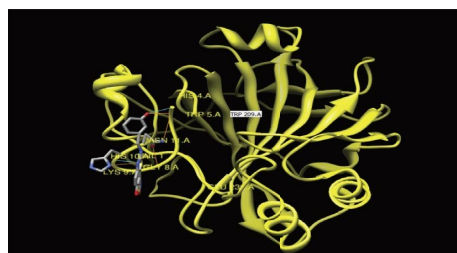


FIGURE 3: Protein-ligand complex of 3BL1 and IIIb.

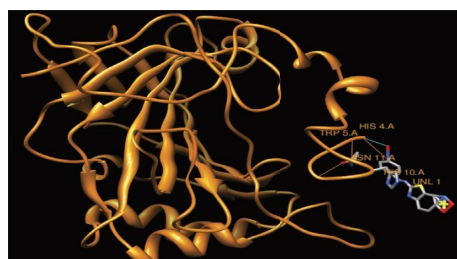


FIGURE 4: Protein-ligand complex of 3BL1 and IIIe.

TABLE 1: Lipinski filtering rule of five.

Compound	Molecular weight	Hydrogen bond donors	Hydrogen bond acceptors	Log p	Molar refractivity
IIIa	322	0	7	1.22	75.45
IIIb	322	0	7	1.15	76.10
IIIc	322	0	7	1.73	76.82
III d	352	0	5	2.10	78.31
IIIe	352	0	5	1.78	78.10
III f	352	0	5	1.78	78.10
III g	341.50	0	6	2.14	74.35
III h	341.50	0	6	2.14	74.35
III i	341.50	0	6	2.14	74.35
Standard	216.00	0	7	0.30	40.97

TABLE 2: Exploration of Molsoft's properties.

Compound	Mol. formula	Mol. weight	HBA	HBD	Mlogp	Mlogs	Mol PSA	Mol volume
IIIa	C ₁₄ H ₁₂ N ₃ O ₃ S ₂	334.03	7	4	3.10	-4.50	85.28	269.20
IIIb	C ₁₄ H ₁₂ N ₃ O ₃ S ₂	334.03	7	4	3.22	-4.78	86.35	269.20
IIIc	C ₁₄ H ₁₂ N ₃ O ₃ S ₂	334.03	7	4	3.22	-4.81	86.35	269.23
III d	C ₁₄ H ₁₁ N ₄ O ₄ S ₂	363.02	8	3	3.03	-5.16	101.81	283.12
III e	C ₁₄ H ₁₁ N ₄ O ₄ S ₂	363.02	8	3	3.15	-5.73	102.11	283.74
III f	C ₁₄ H ₁₁ N ₄ O ₄ S ₂	363.02	8	3	3.15	-5.81	101.11	283.67
III g	C ₁₄ H ₁₁ ClN ₃ O ₂ S ₂	352.00	6	3	4.08	-5.73	68.73	273.35
III h	C ₁₄ H ₁₁ ClN ₃ O ₂ S ₂	352.00	6	3	4.20	-5.84	68.73	275.95
III i	C ₁₄ H ₁₁ ClN ₃ O ₂ S ₂	352.00	6	3	4.20	-5.91	68.73	275.87

TABLE 3: Pass results.

Compound	Carbonic anhydrase inhibition									
	I		II		IV		IX		XII	
	Pa	Pi	Pa	Pi	Pa	Pi	Pa	Pi	Pa	Pi
IIIa	0,012	0,003	—	—	—	—	0,026	0,006	0,048	0,006
IIIb	—	—	0,183	0,004	—	—	—	—	0,045	0,006
IIIc	0,015	0,012	0,015	0,003	—	—	—	—	0,051	0,005
III d	—	—	0,199	0,002	—	—	—	—	0,057	0,005
III e	—	—	0,150	0,003	—	—	0,033	0,005	0,056	0,008
III f	0,019	0,008	0,188	0,002	—	—	—	—	0,064	0,004
III g	0,017	0,002	0,196	0,003	—	—	—	—	0,055	0,001
III h	—	—	0,070	0,004	—	—	0,032	0,005	0,057	0,005
III i	0,015	0,012	0,092	0,003	—	—	—	—	0,057	0,005
Standard	0,418	0,001	0,501	0,001	0,379	0,001	0,628	0,001	0,770	0,000

Here, *Pa*: probability to be active. *Pi*: probability to be inactive.

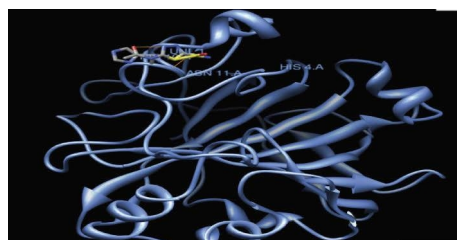


FIGURE 5: Protein-ligand complex of 3BL1 and standard (acetazolamide).

TABLE 4: The molecular docking interactions and the binding energy of 3BL1 compounds.

Ligand	Docking score (kcal/mol)	Number of hydrogen bonds	Key residues	Distance (Å)
IIIb	-5.63	5	HIS 4.A	2.69
			TRP 10.A	3.22
			LYS 4.A	3.35
			HIS 10.A	3.88
			GLY 8.A	—
IIIc	-4.81	0	—	—
III d	-3.95	1	ASN 11.A	3.53
III e	-5.08	3	HIS 10.A	3.24
			ASN 11.A	2.87
			HIS 4.A	3.53
			TRP 5.A	—
III f	-4.56	0	—	—
Acetazolamide	-3.38	2	HIS 10.A	2.80
			ASN 11.A	2.55

EtOH-Ethanol, GAA-Glacial acetic acid.

3. Results

3.1. In Silico Analysis. The results of Lipinski filtering rule of five, Molsoft's properties, PASS results are shown in Tables 1–3.

3.2. Docking Analysis. This approach, known as docking, is used to establish the exact binding conformation and

orientation of ligand molecules into the active regions of proteins using computer simulation. Nine benzothiazole compounds were synthesized, and the standard (acetazolamide) was docked using AutoDock 4.2.6 against carbonic anhydrase II.

The finest conformers have been identified via the use of the Lamarckian genetic process. During each run of the evolutionary algorithm, the population size was set at 150 persons at random, and the maximum number of energy evaluations was restricted to 2,500,000 for each run. All active

TABLE 5: Physical data for synthesized compounds.

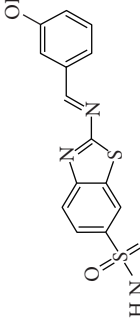
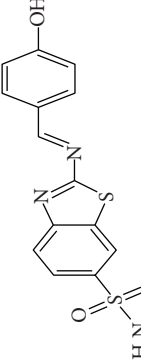
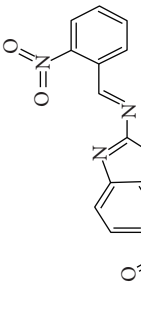
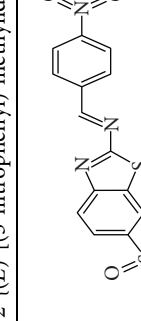
Code	Compounds	Mol Wt	Mol. Formula	Solubility	m.p (°C)	% Yield	R_f value
IIIa	 2-[(E)-[(2-hydroxyphenyl)methylidene]amino]-1,3-benzothiazole-6-sulfonamide	333.30	$C_{14}H_{11}N_3O_3S_2$	$CHCl_3$, CH_3OH , C_2H_5OH , DMSO	92–98	55	0.68
IIIb	 2-[(E)-[(3-hydroxyphenyl)methylidene]amino]-1,3-benzothiazole-6-sulfonamide	333.30	$C_{14}H_{11}N_3O_3S_2$	$CHCl_3$, CH_3OH , C_2H_5OH , DMSO	95–100	43	0.55
IIIc	 2-[(E)-[(4-hydroxyphenyl)methylidene]amino]-1,3-benzothiazole-6-sulfonamide	333.30	$C_{14}H_{11}N_3O_3S_2$	$CHCl_3$, CH_3OH , C_2H_5OH , DMSO	95–100	45	0.51
III d	 2-[(E)-[(2-nitrophenyl)methylidene]amino]-1,3-benzothiazole-6-sulfonamide	294.37	$C_{14}H_{11}N_4O_4S_2$	$CHCl_3$, CH_3OH , C_2H_5OH , DMSO	105–109	39	0.59
IIIe	 2-[(E)-[(3-nitrophenyl)methylidene]amino]-1,3-benzothiazole-6-sulfonamide	294.37	$C_{14}H_{11}N_4O_4S_2$	$CHCl_3$, CH_3OH , C_2H_5OH , DMSO	101–105	45	0.82
III f	 2-[(E)-[(4-nitrophenyl)methylidene]amino]-1,3-benzothiazole-6-sulfonamide	294.37	$C_{14}H_{11}N_4O_4S_2$	$CHCl_3$, CH_3OH , C_2H_5OH , DMSO	95–100	48	0.64

TABLE 5: Continued.

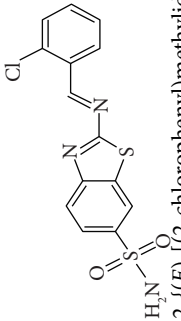
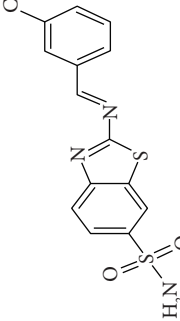
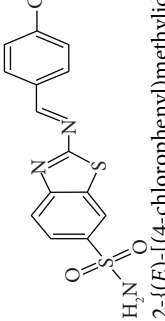
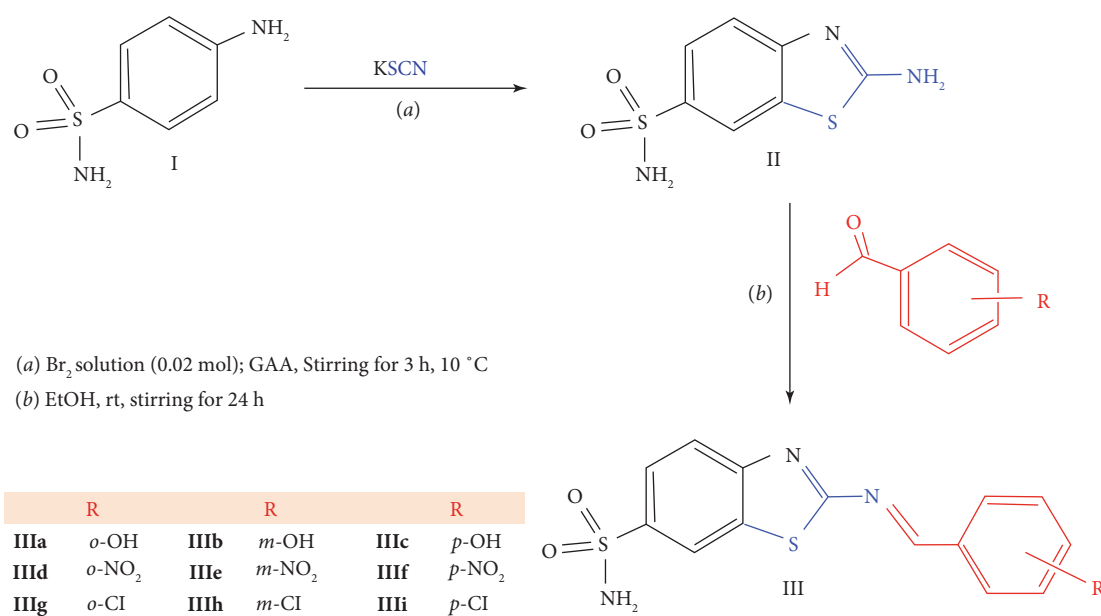
Code	Compounds	Mol Wt	Mol. Formula	Solubility	m.p (°C)	% Yield	R_f value
IIIg	 2-((E)-[(2-chlorophenyl)methylidene]amino)-1,3-benzothiazole-6-sulfonamide	294.37	$C_{14}H_{11}ClN_3O_2S_2$	$CHCl_3$, CH_3OH , C_2H_5OH , DMSO	120–125	39	0.8
IIIh	 2-((E)-[(3-chlorophenyl)methylidene]amino)-1,3-benzothiazole-6-sulfonamide	294.37	$C_{14}H_{11}ClN_3O_2S_2$	$CHCl_3$, CH_3OH , C_2H_5OH , DMSO	130–135	39	0.62
IIIi	 2-((E)-[(4-chlorophenyl)methylidene]amino)-1,3-benzothiazole-6-sulfonamide	294.37	$C_{14}H_{11}ClN_3O_2S_2$	$CHCl_3$, CH_3OH , C_2H_5OH , DMSO	125–130	39	0.64

TABLE 6: Diuretic activity of IIIb and IIIe derivatives.

Treatment	Dose	Urinary volume (ml)	Urinary excretion (Vo/Vt) X 100	Diuretic action UEt/UEc	Diuretic activity DAT/DAu	Lipschitz value
Control	0.9% NaCl 25 ml/kg	2.2 ± 0.25	68.75	—	—	—
Urea	1 gm/kg	4.1 ± 0.45***	128.12	1.86	—	1.67
Acetazolamide	25 mg/kg	3.56 ± 0.45***	114.83	1.67	0.89	0.89
	45 mg/kg	4.21 ± 0.45***	126.96	1.84	0.98	1.84
IIIb	25 mg/kg	3.7 ± 0.31***	112.12	1.63	0.87	0.87
	45 mg/kg	4.25 ± 0.21***	128.18	1.85	0.99	1.04
IIIe	25 mg/kg	3.81 ± 0.35***	119.06	1.73	0.93	0.92
	45 mg/kg	4.43 ± 0.26***	134.24	1.95	1.04	1.95

UEt = Urinary excretion in the test group; UEc = Urinary excretion in the control group; DAT = Diuretic action in the test group; DAu = Diuretic action of urea. * $P < 0.05$ (Dunnett's multiple comparison test) when using one way ANOVA. *** $P < 0.001$, ** $P < 0.01$, * $P < 0.05$ (Dunnett's multiple comparison test) when using one way ANOVA.



SCHEME 1: Synthesis of novel benzothiazole derivatives.

site residues in stiff macromolecules were included in the computations since the grid box size was increased to allow for all active site residues. To fit all of the active site residues, the grid box was centered at 9.323 Å × 1.691 Å × 15.842 Å and its X, Y, and Z co-ordinates were all changed to 90, 90, 90 to accommodate the active site residues.

Docking tests demonstrated that the top 5 ligands had the lowest affinity for the target protein carbonic anhydrase II, when compared to all other ligands evaluated in this study. The binding energy (Kcal/mol) and the number of hydrogen bonds formed with active site areas of the protein were measured and analyzed in the study of protein-ligand interactions. With the use of the Chimera 1.13.1 viewer, the docking contacts between the six ligands and carbonic anhydrase protein were seen and are shown in Figures 2–5. The final docked confirmation for the different ligands is shown in Tables 4–7 in accordance with the binding energy,

the number of hydrogen bonds formed, the bond distance, and the interacting residues. Third, **IIIb** and acetazolamide had the lowest binding energy, with a docking score of −5.63 Kcal/mol (creating four hydrogen bonds with HIS) and −3.38 Kcal/mol (forming two hydrogen bonds with each of HIS and ASN), respectively.

3.3. Experimental. Compound **IIIb**: FTIR (cm⁻¹): 3376 (O-H str), 3154 (aromatic C-H str), 2923 (aliphatic C-H str), (C=N str), 1078 (C-N str), 1459 (C=C str), 1376 (SO₂NH₂ str), 721 (disubstituted benzene), 829 cm⁻¹ (asymmetrically substituted benzene) (Figure 6).

¹H NMR (δ ppm, DMSO): 2.4 (s, 1H, C-H); 6.9 (d, 1H, ArH); 7.0–7.4 (m, 3H, ArH); 7.8–8.0 (2d, 2H, ArH); 7.9 (d, 1H, ArH); 8.4 (s, 1H, ArH); 10.0 (s, 2H, NH₂) (Figure 7).

TABLE 7: Electrolyte excretion of IIIb and IIIe derivatives.

Treatment [†]	Dose	Electrolyte Excretion Index	
		Na ⁺	K ⁺
Control	0.9% NaCl	125.83 ± 1.16	43.33 ± 1.86
Urea	1 gm/kg	144.83 ± 1.94***	54.55 ± 3.14**
Acetazolamide	25 mg/kg	193.83 ± 3.18***	76.33 ± 3.66**
	45 mg/kg	283.00 ± 2.75***	136.83 ± 3.24***
IIIb	25 mg/kg	215.33 ± 3.14***	84.5 ± 3.01**
	45 mg/kg	282.83 ± 2.41***	144.33 ± 1.63***
IIIe	25 mg/kg	188.83 ± 3.70***	69.33 ± 2.16**
	45 mg/kg	277.5 ± 2.48***	123.66 ± 1.75***

Results are presented as mean standard error of the mean ($n = 6$), with *** $P < 0.001$, ** $P < 0.01$, * $P < 0.05$ (Dunnett's multiple comparison test) and one way ANOVA. Na⁺ = sodium index, K⁺ = potassium index.

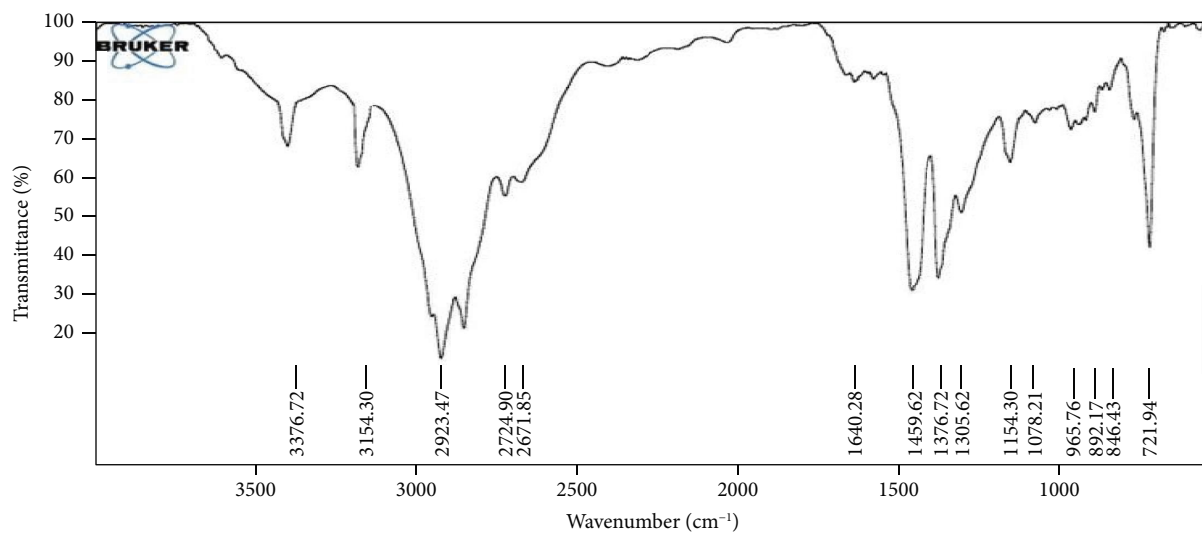
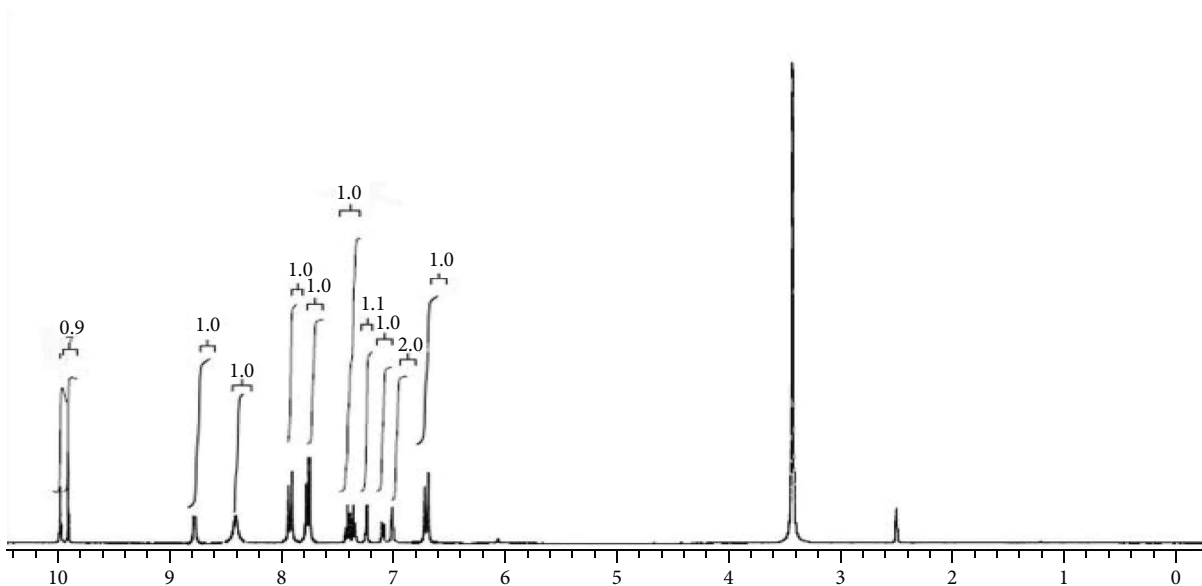


FIGURE 6: IR spectra of compound IIIb.

FIGURE 7: ¹H-NMR spectra of compound IIIb.

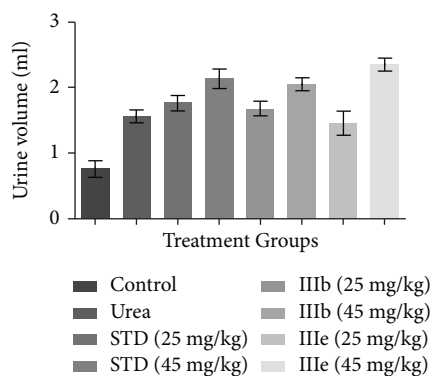
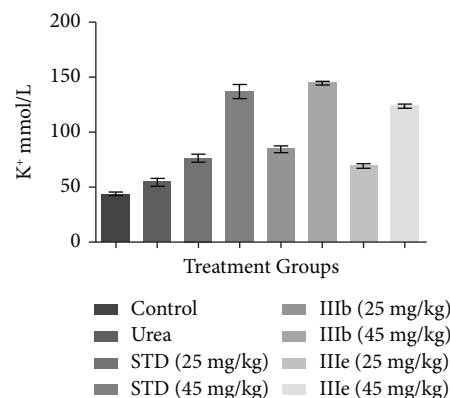
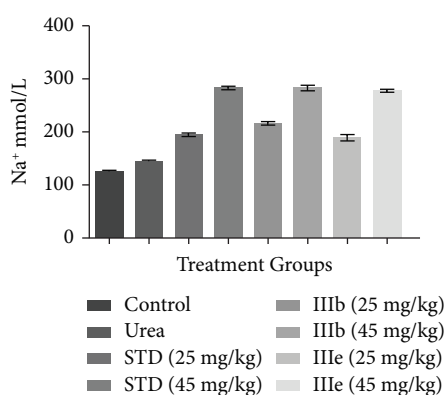


FIGURE 8: Diuretic activity in rats: a dose-response study.

FIGURE 10: Electrolyte excretion (K⁺ mmol/L) in rats.FIGURE 9: Electrolyte excretion (Na⁺ mmol/L) in rats.

3.4. Diuretic Activity. The *in vivo* diuretic activity of the benzothiazole derivatives was determined using a conventional technique against male Wistar rats, and the results were compared to those of the reference compound (Tables 6–7 and Figures 8–10).

Both the synthesized compounds (**IIIb**) are found to be equipotent and (**IIIe**) is more potent than the standard drug (acetazolamide).

4. Discussion

Based on the results of Lipinski rule of five, the compounds synthesized were obeying Lipinski rule of 5. PASS values suggesting that all the synthesized compounds obey the PASS values. The standard (acetazolamide) has action nonselectively on all the sub classes of carbonic anhydrase enzyme. The molecules **IIIb**, **IIIc**, **IIIId**, **IIIe**, **IIIf**, and **IIIg** have $P_a > 0.1$ primarily acting on carbonic anhydrase II, but the standard with $P_a > 0.3$ acting on all the subtypes of the enzyme. Toxicity (tumorigenic and reproductive effects) is present in the normal medicine, but not in the synthesized molecules except for **IIIId** and **IIIIf**, according to the OSIRIS molecular property explorer. The length of the hydrogen bonds produced with the interacting residues in the docking study findings reveals that the bonding was excellent for all of the ligands tested. The PDB sum predicted most of the

important residues presented in Table 4 to be active site residues. All of the ligands have docking contacts with the protein carbonic anhydrase II, according to the docking score. This research used ligands having diuretic activity, which may have a distinct mechanism of action. Using molecular docking simulations, this research found that the **IIIb** and **IIIe**, block carbonic anhydrase II.

All of the more modern benzothiazole derivatives were created in the laboratory by mixing a number of different chemical reagents together. Hydroxyl derivatives were more productive in this case. TLC and melting points of the synthesized compounds differed significantly from those of the first stage product. One component, **IIIb**, was purified using column chromatography and characterized using spectroscopic methods including FTIR and ¹H NMR after it was produced and recrystallized from ethanol.

5. Conclusion

The results of the evaluation of diuretic activity indicated that the compound **IIIb** having urinary excretion, diuretic action, diuretic activity, and Lipschitz values higher than the standard drug which indicate that it is more potent than the standard. From Table 7 and Figures 8 and 9, it is evident that the sodium excretion is more and potassium excretion is moderate to that of the standard and urea-treated groups at 45 mg/kg dose.

Data Availability

All data used to establish the conclusions of this study are integrated into the article.

Conflicts of Interest

The authors declare that they have no conflicts of interest.

Acknowledgments

The authors extend their appreciation to the Deanship of Scientific Research at King Khalid University (KKU) for funding this work through the Research Group Program Under the Grant Number (R.G.P.1/256/43). This research received support by the Taif University Researchers

Supporting Project, number (TURSP-2020/242), Taif University, Taif, Saudi Arabia.

References

- [1] H. Rang, *Rang and Dale's Pharmacology*, Elsilver Co, London, UK, 6th edition, 2007.
- [2] M. E. Ernst and M. A. Fravel, "Thiazide and the thiazide-like diuretics: review of hydrochlorothiazide, chlorthalidone, and indapamide," *American Journal of Hypertension*, vol. 35, no. 7, pp. 573–586, 2022.
- [3] H. Smith, "Diuretics: a review for the pharmacist," *SA Pharmaceutical Journal*, vol. 81, pp. 18–21, 2014.
- [4] D. Gandhi, P. Kalal, P. Prajapat, D. K. Agarwal, and S. Agarwal, "Diversity oriented synthesis of 4H-pyrimido [2, 1-b] benzothiazole derivatives via biginellis reaction: a review," *Combinatorial Chemistry & High Throughput Screening*, vol. 21, no. 4, pp. 236–253, 2018.
- [5] Q. Sun and X. Bao, "Facile preparation of dihydro-1, 4-benzothiazine derivatives via oxidative ring-expansion of 2-aminobenzothiazoles with olefins," *Chemical Communications*, vol. 58, no. 13, pp. 2216–2219, 2022.
- [6] Ş. Karaca, D. Osmaniye, B. N. Sağlık et al., "Synthesis of novel benzothiazole derivatives and investigation of their enzyme inhibitory effects against Alzheimer's disease," *RSC Advances*, vol. 12, no. 36, pp. 23626–23636, 2022.
- [7] F. Piscitelli, C. Ballatore, and A. B. Smith, "Solid phase synthesis of 2-aminobenzothiazoles," *Bioorganic & Medicinal Chemistry Letters*, vol. 20, no. 2, pp. 644–648, 2010.
- [8] V. Jaitak, V. Jaitak, and K. Kaur, "Thiazole and related heterocyclic systems as anticancer agents: a review on synthetic strategies, mechanisms of action and SAR studies," *Current Medicinal Chemistry*, vol. 29, no. 29, pp. 4958–5009, 2022.
- [9] N. Arul Murugan, G. Ruba Priya, G. Narahari Sastry, and S. Markidis, "Artificial intelligence in virtual screening: models versus experiments," *Drug Discovery Today*, vol. 27, no. 7, pp. 1913–1923, 2022.
- [10] M. P. S. Murkute, R. S. Raut, N. P. Kathar, G. S. Sanap, and R. G. Gaikwad, *Brief Introduction to In-Silico Drug Discovery Process and Virtual Screening Method; Ubiquitination Regulator in Cancer: A Review*, 2022.
- [11] D. B. Kitchen, H. Decornez, J. R. Furr, and J. Bajorath, "Docking and scoring in virtual screening for drug discovery: methods and applications," *Nature Reviews Drug Discovery*, vol. 3, no. 11, pp. 935–949, 2004.
- [12] X. Chen, H. Li, L. Tian, Q. Li, J. Luo, and Y. Zhang, "Analysis of the physicochemical properties of acaricides based on Lipinski's rule of five," *Journal of Computational Biology*, vol. 27, no. 9, pp. 1397–1406, 2020.
- [13] N. Flores-Holguín, J. Frau, and D. Glossman-Mitnik, "Chemical reactivity properties, drug-likeness features and bioactivity scores of the cholecystokinin peptide hormone," *Computational Molecular Bioscience*, vol. 09, no. 02, pp. 41–47, 2019.
- [14] E. Perola and P. S. Charifson, "Conformational analysis of drug-like molecules bound to proteins: an extensive study of ligand reorganization upon binding," *Journal of Medicinal Chemistry*, vol. 47, no. 10, pp. 2499–2510, 2004.
- [15] Ö.-M. S. Y. A. Doğan-Sadin, S. Özdemir, M. S. Yalcin, H. Sari, and Y. Nural, "Naphthoquinone-thiazole hybrids bearing adamantane: synthesis, antimicrobial, DNA cleavage, anti-oxidant activity, acid dissociation constant, and drug-likeness," *Journal of Research In Pharmacy (Online)*, vol. 25(3), no. 25(3), pp. 292–304, 2021.
- [16] G. O. Oduselu, O. O. Ajani, Y. U. Ajamma, B. Brors, and E. Adebisi, "Homology modelling and molecular docking studies of selected substituted Benzo [d] imidazole-1-yl (methyl) benzimidamide scaffolds on Plasmodium falciparum adenylosuccinate lyase receptor," *Bioinformatics and Biology Insights*, vol. 13, Article ID 117793221986553, 2019.
- [17] A. Daina, O. Michielin, and V. Zoete, "SwissADME: a free web tool to evaluate pharmacokinetics, drug-likeness and medicinal chemistry friendliness of small molecules," *Scientific Reports*, vol. 7, pp. 42717–42813, 2017.
- [18] A. Husain, D. Madhesia, M. Rashid, A. Ahmad, and S. A. Khan, "Synthesis and in vivo diuretic activity of some new benzothiazole sulfonamides containing quinoxaline ring system," *Journal of Enzyme Inhibition and Medicinal Chemistry*, vol. 31, no. 6, pp. 1682–1689, 2016.
- [19] J. K. Malik, F. Manvi, B. Nanjwade, S. Singh, and P. Purohit, "Review of the 2-amino substituted benzothiazoles: different methods of the synthesis," *Der Pharmacia Lettre*, vol. 2, pp. 347–359, 2010.
- [20] R. Amin, C. Quispe, J. Herrera-Bravo et al., "Ethnopharmacological-Based validation of *Polyalthia suberosa* leaf extract in neurological, hyperalgesic, and hyperactive gut disorders using animal models," *Evidence-based Complementary and Alternative Medicine*, vol. 2022, Article ID 1345006, 9 pages, 2022.
- [21] M. N. Bhoi, M. A. Borad, N. K. Panchal, and H. D. Patel, "2-Aminobenzothiazole containing novel Schiff bases derivatives: search for new Antibacterial agents," *International Letters of Chemistry, Physics and Astronomy*, vol. 53, pp. 106–113, 2015.
- [22] C. A. Lipinski, F. Lombardo, B. W. Dominy, and P. J. Feeney, "Experimental and computational approaches to estimate solubility and permeability in drug discovery and development settings," *Advanced Drug Delivery Reviews*, vol. 23, no. 1-3, pp. 3–25, 1997.
- [23] K. Kailas, J. Sheetal, P. Anita, and H. Apoorva, "Four synthesis methods of schiff base ligands and preparation of their metal complex with Ir and antimicrobial investigation," *World Journal of Pharmacy and Pharmaceutical Sciences*, vol. 5, pp. 1055–1063, 2016.
- [24] S. Parasuraman, "Prediction of activity spectra for substances," *Journal of Pharmacology and Pharmacotherapeutics*, vol. 2, no. 1, pp. 52–53, 2011.
- [25] T. Lengauer and M. Rarey, "Computational methods for biomolecular docking," *Current Opinion in Structural Biology*, vol. 6, no. 3, pp. 402–406, 1996.
- [26] H. G. Vogel, W. H. Vogel, H. G. Vogel, G. Müller, J. Sandow, and B. A. Schölkens, *Drug Discovery And Evaluation: Pharmacological Assays*, Springer, Berlin/Heidelberg, Germany, 1997.

Research Article

The Effect of Cytotoxicity and Antimicrobial of Synthesized CuO NPs from Propolis on HEK-293 Cells and *Lactobacillus acidophilus*

Yasamin Seyyed Hajizadeh,¹ Ebrahim Babapour,¹ Naser Harzandi,¹ Mohsen Yazdanian ,² and Reza Ranjbar ³

¹Department of Microbiology, Karaj Branch, Islamic Azad University, Karaj, Iran

²Research Center for Prevention of Oral and Dental Diseases, Baqiyatallah University of Medical Sciences, Tehran, Iran

³Molecular Biology Research Center, Systems Biology and Poisonings Institute, Baqiyatallah University of Medical Sciences, Tehran, Iran

Correspondence should be addressed to Reza Ranjbar; ranjbarre@yahoo.com

Received 12 September 2022; Revised 11 October 2022; Accepted 27 January 2023; Published 9 February 2023

Academic Editor: Fernanda Tonelli

Copyright © 2023 Yasamin Seyyed Hajizadeh et al. This is an open access article distributed under the Creative Commons Attribution License, which permits unrestricted use, distribution, and reproduction in any medium, provided the original work is properly cited.

Background. Drug resistance is currently possible anywhere in the world. Due to the discovery of antimicrobials, medicine, and health have made tremendous advances over the past several decades. **Aim.** This research evaluated the antimicrobial and cytotoxicity effects of green synthesis of copper oxide nanoparticles (CuO NPs) on *Lactobacillus acidophilus* and human embryonic kidney 293 cells (HEK). **Method and Materials.** Propolis was sampled and extracted. Green synthesis of CuO NPs was synthesized and characterized using SEM, TEM, DLS, BET, and zeta potential methods. *L. acidophilus* (ATCC 4356) was used, and the antimicrobial tests were carried out at different concentrations ($10 \geq$ mg/ml). Moreover, the cytotoxicity was evaluated using an MTT assay on human embryonic kidney 293 cells (HEK). **Results.** Synthesized CuO NPs using propolis extracts from Khalkhal (sample 1) and Gillan (sample 2) showed -13.2 and -14.4 mV, respectively. The hydrodynamic sizes of well-dispersed samples 1 and 2 were 3124.9 nm and 1726.7 nm, respectively. According to BET analysis, samples 1 and 2 had 5.37 and 8.45 m²/g surface area, respectively. The surface area was decreased due to the addition of propolis extract, and the pore size was increased. CuO NPs of samples 1 and 2 were visible on SEM images with diameters ranging from 75 to 145 nm and 120 to 155 nm, respectively. Based on TEM analysis, the size of CuO particles was increased in samples 1 and 2. CuO NPs particles had narrow size distributions with evenly dispersed NPs on all sides. The cell viability of the CuO NPs of samples 1 and 2 after 24, 48, and 72 hours was greater than 50%. As a result of the MIC and MBC tests, it was determined that samples 1 and 2 had the same effect against *L. acidophilus* (0.0024 mg/ml). Biofilm formation and degradation of sample 1 were more efficient against *L. acidophilus*. **Conclusion.** There was no evidence of cytotoxicity in the samples. In addition, results showed that the green synthesized CuO NPs from Khalkhal propolis were effective against *L. acidophilus*. Thus, the green synthesized CuO NPs from Khalkhal propolis were the best candidates for clinical application.

1. Introduction

Microorganisms in the mouth can destroy teeth. Throughout the world, this disease affects many generations. In recent years, silver metal has been replaced with resin restorations due to the advent of silver amalgam treatments in dentistry in the 19th century [1]. During the last few

decades, antibiotics have made considerable advances in the medical field. An emerging phenomenon called antimicrobial resistance could impede international health and sustainable development goals by compromising therapeutic strategies. As a result of AMR, countries and continents have been affected more rapidly than ever, making it one of the most severe public health crises ever. Antibiotic Stewardship

program activities include ensuring appropriate diagnostics and treatment of drug-resistant infections and appropriate use of antibiotics judiciously [2]. There is no doubt that nanotheranostics represents an advancement in nanomedicine. Nanomaterials and nanotechnology can be used to improve medicinal Efficacy. A unique physicochemical property, targeted delivery, and reduced chance of developing resistance make NPs a popular alternative to antibiotics. Metallic NPs are most commonly reported as alternative antibacterial agents [2–5]. *Lactobacillus* is acidogenic bacteria that cause dental caries. Children and adults suffer from pain, structural damage to their teeth, and eventual tooth loss due to the loss of mineralized tissues. *Lactobacillus* is the most common bacteria that cause periodontal diseases and cause inflammation, and infection [6–11]. An arsenal of redox potentials is found in plant extracts. NPs with defined sizes can be produced by biogenic synthesis using phytochemical compounds as stabilizers. Propolis is used in traditional medicine for its biological properties. The antioxidative, anti-inflammatory, and antibacterial properties of propolis are noteworthy. Propolis exhibits antiproliferative and antitumor properties *in vitro* and *in vivo*. It depends on the region, climate, and extraction season. Because propolis contains polyphenolic acids, flavonoids, and terpenoids, it can produce gold NPs [12–18]. The cost of manufacturing metallic NPs can be reduced by capping and reducing metallic NPs with biological components. Since they do not require excessive pressure or energy, they are environmentally friendly and energy-efficient [18–21]. NPs can be manufactured from medicinal plants. Allium sativum, Aleo vera, and Punica granatum have been used to synthesize copper NPs [22, 23]. This research aimed to synthesize the CuO NPs using propolis extracts and evaluate their antibacterial and cytotoxicity on *Lactobacillus acidophilus* and HEK-293 cells, respectively.

2. Method and Material

2.1. Materials. Propolis was collected from Gillan and Khalkhal (Figure 1). To synthesize CuO NPs, the following materials need to be used: copper sulfate pentahydrate ($\text{CuSO}_4 \cdot 5\text{H}_2\text{O}$) (Sigma Aldrich, Co., USA) and absolute ethanol (Merck, Germany). This experiment used reagents purchased from Merck, Germany; none of them were purified before use.

2.2. Preparation of Propolis Extract. Ground samples were prepared and frozen (-20°C) for a while. In this study, raw propolis samples were extracted (by stirring them in a tenfold amount of ethanol (70%) for three days in a dark environment at room temperature) to quantify their ethanol content. To remove waxes and other less soluble substances from the suspensions, they were filtered (Whatman paper, No.1) to make sure that all waxes and other less soluble substances were removed from the suspensions. It was necessary to repeat this procedure three times to get the desired results. The freeze-dried extract solution was obtained for the next steps [24].



FIGURE 1: Two propolis samples were collected from Khalkhal, Ardabil province, and Gillan province, Iran.

2.3. Green Biosynthesized Copper NPs. To synthesize CuO NPs, the procedure was to dissolve 1 mg of extract in deionized water to form a solution and then adjust the pH of this solution to 8 by adding NaOH to form a solution. A solution of copper sulfide (6 mM) was slowly added to 100 ml of the extract solution while stirring with a rotation speed of 1,000 rpm. The samples were then placed in a flask and stirred (24 h, 37°C to 40°C) in the dark at a temperature between 37°C and 40°C in the dark. After the colored mixture (dark brown) had been obtained, it was centrifuged at 13,000 rpm (15 min, 25°C) to obtain the colored mixture (dark brown). A deionized water wash was performed on the pellet twice to ensure that all residues were removed from the extract. A lyophilized precipitate was then stored to be analyzed in the future.

2.4. Zeta Potential Analysis. Zeta Potential analysis was used to detect the hydrodynamic size polydispersity index and the size polydispersity index of the synthesized NPs. Particle sizes were evaluated under an angle of 90 degrees at 25°C .

2.5. DLS Analysis. This study used the DLS method to size metal oxide NPs (measured in terms of hydrodynamic radius) according to the range sizing method. An open capillary cell was used in a 37°C water bath, and a disposable folded capillary cell was used to measure the particle sizes of the dispersions after they had been prepared using a disposable folded capillary cell.

2.6. BET Analysis. As a part of the investigation, the surface area of NPs under vacuum was determined using the Brunauer–Emmett–Teller (BET). As part of the surface area measurement, a 2-hour vacuum degassing of the sample was carried out at 120°C .

2.7. SEM Analysis. To determine the structure and morphology structure of the NPs, the SEM examination was carried out. As part of the SEM studies, approximately 25 μL of NPs were applied to the CuO stub, and the results were evaluated. Using a scanning electron microscope, photographs of the samples were taken [25]. Approximately 10 kV of accelerating voltage was used with a working distance of approximately 3 mm. The brightness and contrast correction also resulted in clear and distinguishable images that could be displayed. The lengths of the measurement scales, 500 nm and 20 μm , were calibrated using the NISTRM for calibration purposes.

2.8. TEM Analysis. The shapes of the CuO NPs were observed using TEM imaging based on suspensions induced by propolis-mediated suspensions accelerated at 200 KV and tilted at X-tilt $\pm 60^\circ$. A copper grid coated with carbon was used as a platform for the droplet of NPs solutions to achieve this goal. A specimen holder was used to mount the grid once it had dried, and a few minutes later, it was mounted on the specimen holder for drying. The TEM image of the selected area of the sample was overlaid with the selected area's diffraction pattern to clarify the sample's lattice pattern and crystallite size [26].

2.9. Cytotoxicity Assay. Biosynthesized NP solutions were sonicated before using in any experiments. The NPs were sterilized using UV light. In the culture of the human embryonic kidney 293 cells (HEK), 100 U/mL penicillin, 10% fetal bovine serum (Himedia), 100 U/mL penicillin, and 2 mM L-glutamine were used. The cells were maintained at 70–80% confluency by passage every 2–4 days in a 25 cm^2 flask [27]. Human embryonic kidney 293 cells (HEK) were used to test the green biosynthesized NPs [28–31]. In 96-well plates, 100 μL of cell suspension was filled into each well, containing 10000 cells. A set of parameters was followed during incubation. The concentrations of CuO NPs were 2.5, 5, 10, 25, 50, 75, and 100 $\mu\text{g}/\text{mL}$, and the control group was cell culture. Once the initial model had been dissolved in DMSO, the NPs were dispersed in PBS. After adding the samples, the plates were incubated for 48 hours. A control medium was used without test samples. Each well was incubated for four hours at 37°C with 15 μL of MTT in PBS. We dissolved the formazan crystals in 100 μL of DMSO after removing the MTT medium and the medium containing MTT. 570 nm measurements were taken to determine the absorbance. The cell viability percentage was calculated using the following equation:

$$\text{Cell Viability\%} = \frac{\text{sample}}{\text{control}} \times 100. \quad (1)$$

2.10. Determination of Minimal Inhibitory/Bactericidal Concentrations (MIC/MBC). This experiment used *Lactobacillus acidophilus* (ATCC 4356) as the bacteria. 1.5×10^8 CFU/mL was the final concentration [32]. MICs and MBCs of green synthesized CuO NPs from Khalkhal

(sample 1) and Gillan (sample 2) propolis were determined following the guidelines of the NCCLS. To prepare the nutrient broth medium for dilution, a concentration of 10 mg/mL of CuO NPs was added to the nutrient broth at 10 mg/mL. To create solid nutrient agar plates, solid nutrient agar was used for plating the bacteria. It was determined that an inhibitory concentration was reached when the lowest concentration inhibited bacterial growth. The MBC needs to be determined in a concentration that allows bacterial growth to be inhibited entirely. Our experiments were repeated in equal numbers for each sample. The average growth rate of the bacteria on each plate was calculated based on the average growth rate on each plate [33].

2.11. Biofilm Formation Analysis. In the process of conducting this test, microdilutions were used as a dilution method. It was observed that bacteria were cultured for 24 hours using TSB. TSB containing 1% sucrose was used as the dilution solution, and the suspension was diluted 1 : 100 in the solution. The extracts containing 10 \times MBC were used for this test. To transfer 100 μL of a mixture of bacterial suspension and extract solution to each of the microplate wells, 200 μL of 100 μL of a suspension of pathogenic bacteria was transferred, 100 μL of extract solution, and 100 μL of mouthwash. As a positive control, 0.2% chlorhexidine was added as a solution to 200 μL of bacterial suspension and physiological saline in which bacterial suspension and physiological saline were mixed. During the incubation period of 24 hours, the plate surface was incubated at 37°C in an incubator. Using a buffer containing phosphate and saline, the wells were washed three times with the solution after the contents had been removed from them. It was necessary to do this to remove disconnected cells. In the following step, 200 μL of 33% glycolic acetic acid was added to the wells containing cells that had adhered to the bottom to remove them. After 15 minutes, the optical density at 570 nm of each well of each sample was measured using an ELISA reader, and biofilm formation rates (%) were calculated using the mentioned formula based on the optical density at 570 nm of each sample.

$$\text{The biofilm formation rate} = \frac{\text{Samples (OD)}}{\text{Control (OD)}} \times 100. \quad (2)$$

OD treatments and OD controls are defined as the absorbance at 570 nm in each well after the dissolving solution was added to the well with and without the sample, respectively.

2.12. The Biofilm Degradation Analysis. This test was also conducted to investigate whether microdilution has any destructive effects on biofilms. Microplates were inoculated with bacteria using TSB medium, 3% glucose, and synthetic saliva (McDougall solution) for growth. A biofilm was formed as soon as the remaining culture medium of the culture was discarded. The MBC solution was diluted ten times with the sample solution. To remove the biofilms on the walls of the wells, phosphate buffer was used. After

applying it to them, it took 15 minutes for the walls to become saturated with 1% violet crystal. Sterile solutions of water mixed with 95% alcohol were used to clean the wells, and three rinses of sterile water were used after each. After the suspension was transferred from one microplate to another, it was incubated for 45 minutes before the new microplate was used. Using a microplate reader at a wavelength of 570 nm, we measured the optical density of the suspension in each well to determine the extent of degradation of the biofilm. The positive control was chlorhexidine 0.2%. Through the use of the equation mentioned, we were able to calculate the percentage rate of biofilm degradation using the following equation [34]:

$$\text{The biofilm degradation rate} = 100 - \left(\frac{\text{Samples (OD)}}{\text{Control (OD)}} \right) \times 100. \quad (3)$$

OD treatments and OD controls are defined as the absorbance at 570 nm in each well after the dissolving solution was added to the well with and without the sample, respectively.

2.13. Statistical Analysis. It was performed independently in triplicates for each of the tests. A one-way ANOVA test (SPSS statistics model 20) was used to compare the means among the groups, and Tukey's post hoc test allowed further comparisons. The significance level was P value <0.05 .

3. Results

3.1. Characterization Results. A UV-visible spectrophotometer was used in a previous study and performed surface plasmon resonance measurements on CuO NPs. In UV-Vis spectra of CuO NPs prepared from propolis (Khalkhal) extract, a characteristic peak at 385 nm can be seen on the spectrum. As a result of further UV-Vis spectrophotometry investigation into CuO NPs using propolis extract (Gillan), peaks are observed at 243, 292, and 350 nm. CuO NPs were analyzed using XRD techniques using extracts of propolis (Khalkhal), resulting in crystallographic planes of face-centered cubic (FCC) with peaks of diffraction around $2\theta = 35.74^\circ$, 39.04° , and 49.04° . The diffraction peaks of CuO NPs using extracts of propolis (Gillan) were observed around $2\theta = 25.54^\circ$, 26.69° , 38.79° , and 48.84° . The Khalkhal propolis extract FTIR spectrum showed a sharp peak at 3422 cm^{-1} due to free hydroxyl groups and their intramolecular and intermolecular hydrogen bonds. Sharp peaks at 2925, 1637, and 1515 to 1076 cm^{-1} were associated with C=O and C=C aromatic stretching frequencies. CuO NP monoclinic phase exhibits an absorption band of 602 cm^{-1} . As a result of free hydroxyl groups and their intramolecular and intermolecular H-bonds, CuO NPs of the Gillan propolis extract spectrum also peak at 3410 cm^{-1} . CSp3-H and aromatic stretching frequencies of C=O and C=C were related to the peaks at 2920, 1614, and 1515 to 1057 cm^{-1} . An absorption band of 603 cm^{-1} was observed in the monoclinic phase of CuO NPs [35].

3.2. Zeta Potential DLS Analysis. CuO NPs produced from Khalkhal propolis extract (sample 1) showed a zeta potential of -13.2 mV . In contrast, the produced CuO NPs from Gillan propolis extract (sample 2) had a zeta potential of -14.4 mV (Figure 2). As a result of using the sonication method provided by the National Institute of Standards and Technology (NIST), the CuO NPs were separated from CuO NPs synthesized from Khalkhal (sample 1) and Gillan propolis extracts (sample 2); however, there was no noticeable difference between the well-synthesized CuO NPs synthesized using propolis extract and those synthesized using propolis extracts. For well-dispersed samples 1 and 2, it was found that the hydrodynamic sizes were 3124.9 nm and 1726.7 nm , respectively, based on DLS data (Figure 3).

3.3. BET Evaluation. Table 1 shows that the amount of precursor used in the Brunauer–Emmett–Teller (BET) process determines the system's surface area. As a result of the synthesized CuO NPs using different extracts of propolis, it was found that they had a surface area of 5.37 to $8.45 \text{ m}^2/\text{g}$ for samples 1 and 2, respectively. Propolis extract increased the pore size and decreased the surface area.

3.4. SEM and TEM Evaluation. Images obtained from SEM micrographs of the synthesized CuO NPs using propolis extract showed that the crystallization structure of CuO NPs synthesized from propolis extract was quite poly-disperse and similar to anatase phase CuO crystallites. As a result of the experiments in sample 1 (Khalkhal), NPs with diameters ranging from 75 to 145 nm were observed. There were also NPs ranging in diameter between 120 and 155 nanometers in sample 2. Based on the diameter of the propolis extracts from Gillan and Khalkhal, it was possible to compare the extracts based on their diameters (Figure 4). As can be seen in Figure 4, green CuO NPs were biosynthesized with propolis extracts and taken from Khalkhal and Gillan. In part, the increase in CuO particle size can be attributed to the green biosynthesis among samples 1 and 2. It is important to note that CuO NP particles had narrow sizes and were uniformly dispersed throughout all sides of the particle.

3.5. Cell Viability Evaluation. Various concentrations of samples 1 and 2 NPs were incubated with HEK cells to determine their effect on the cell-cultured cells (CuO NPs concentration: 2.5, 5, 10, 25, 50, 75, and $100 \mu\text{g}/\text{mL}$ and control: cell culture) for 24, 48, and 72 h. To determine the viability of cells, the cytotoxicity test must be performed. As a result of both the dose and time dependence, the number of viable cells was decreased in samples 1 and 2 NPs. It was determined that the cell viability percentages for the HEK cells and the control groups were calculated for 24, 48, and 72 hours. As a result of MTT data analyses, the cell survival rate of both samples was approximately more than 50% during 24, 48, and 72 hours (Figure 5).

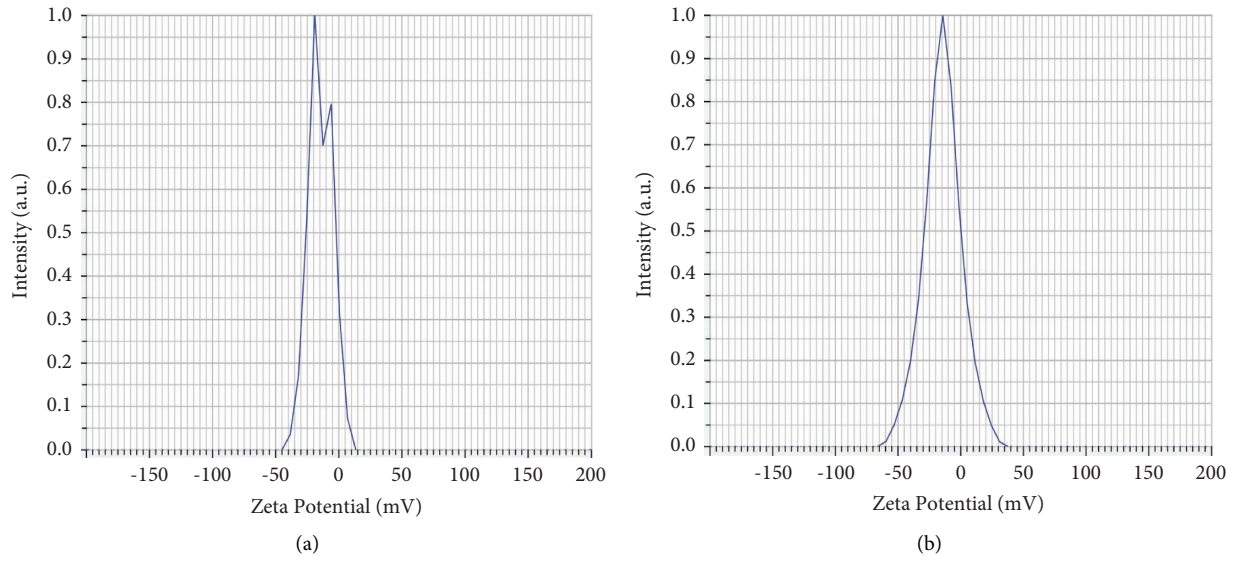


FIGURE 2: Zeta potential of the synthesized CuO of (a) samples 1 (Khalkhal) and (b) sample 2 (Gillan).

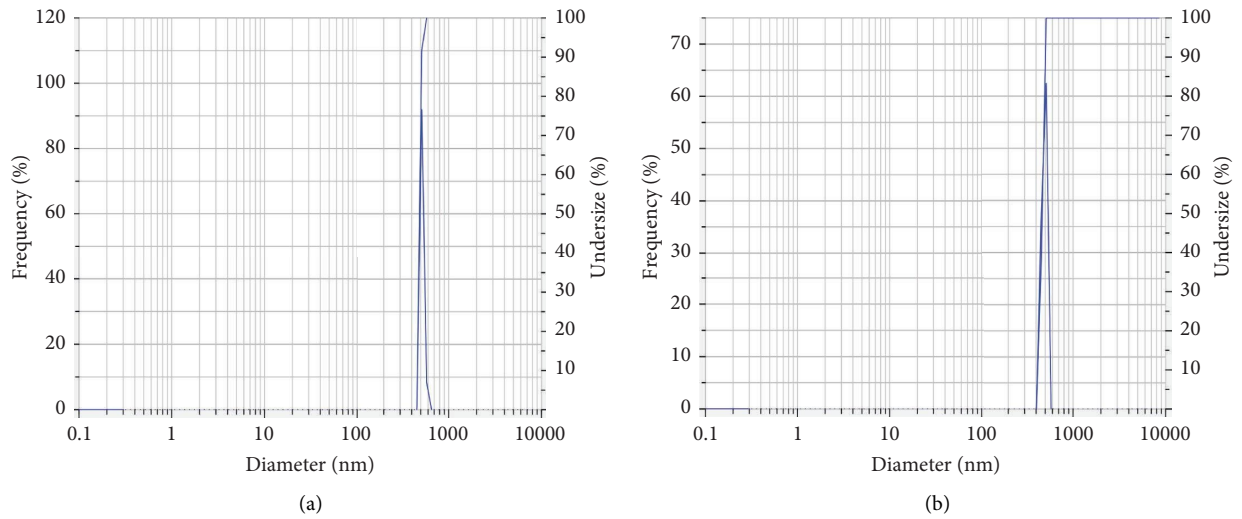


FIGURE 3: Size distributions of the synthesized CuO of (a) samples 1 (Khalkhal) and (b) sample 2 (Gillan).

TABLE 1: The specific surface area of different kinds of green synthesized CuO NPs from Khalkhal (sample 1) and Gillan (sample 2).

Samples	Surface area (m ² /g)
Sample 1	5.3722
Sample 2	8.4537

3.6. Antimicrobial Analysis

3.6.1. MIC and MBC Results. As a result of broth microdilution, MIC of samples 1 and 2 NPs against *L. acidophilus* was determined. The range of MIC values was 0.0024 for *L. acidophilus* (Table 2). As seen in Table 2, levels of MBC were within the range of 0.0024 for *L. acidophilus*.

3.6.2. Biofilm Formation and Degradation Evaluation. It was determined that the samples could prevent biofilm formation using microdilution tests as a method of determining their effectiveness. Table 3 shows the biofilm formation results, and the OD (570 nm) was determined to compare the ODs of treated groups (samples 1 and 2). Sample 2 of the NPs showed the highest levels of biofilm growth compared to sample 1 which showed the highest effect against *L. acidophilus*. Biofilms that had already been formed were also treated with the same method to test the treatment's effects. As a result of the degradation of biofilm, a percentage degradation was calculated (Table 4). There was a significant effect of sample 1 NPs against *L. acidophilus*. Figure 6 shows the biofilm formation and degradation tests of both NPs against *L. acidophilus*.

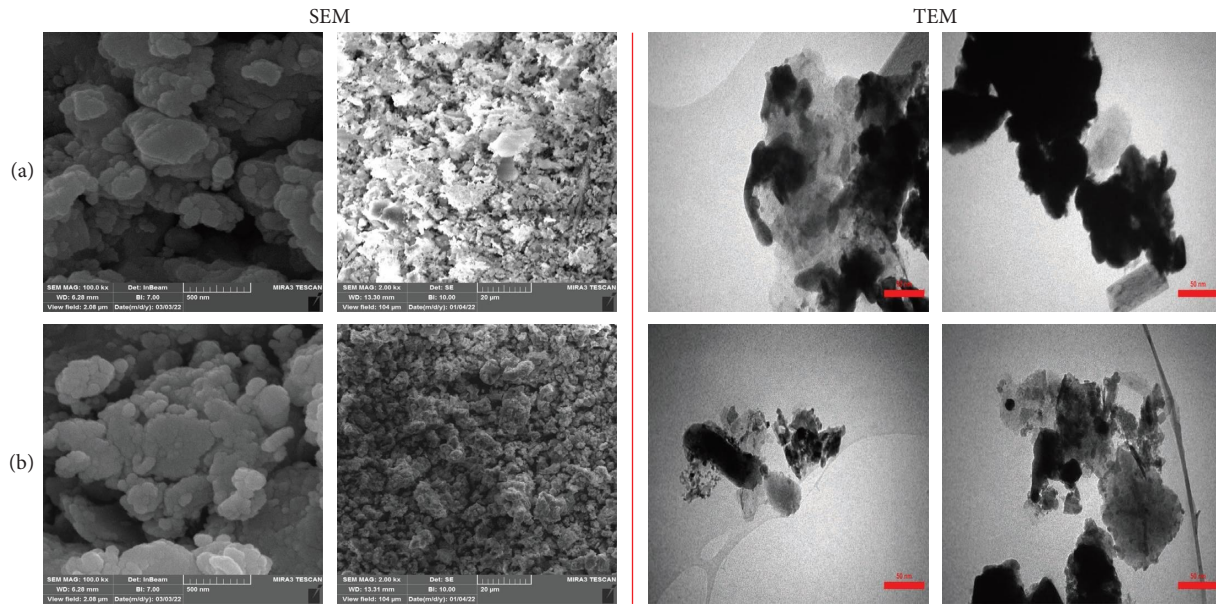


FIGURE 4: SEM (500 nm and 20 μm) and TEM (50 nm) images of the synthesized CuO NPs of (a) samples 1 (Khalkhal) and (b) sample 2 (Gillan).

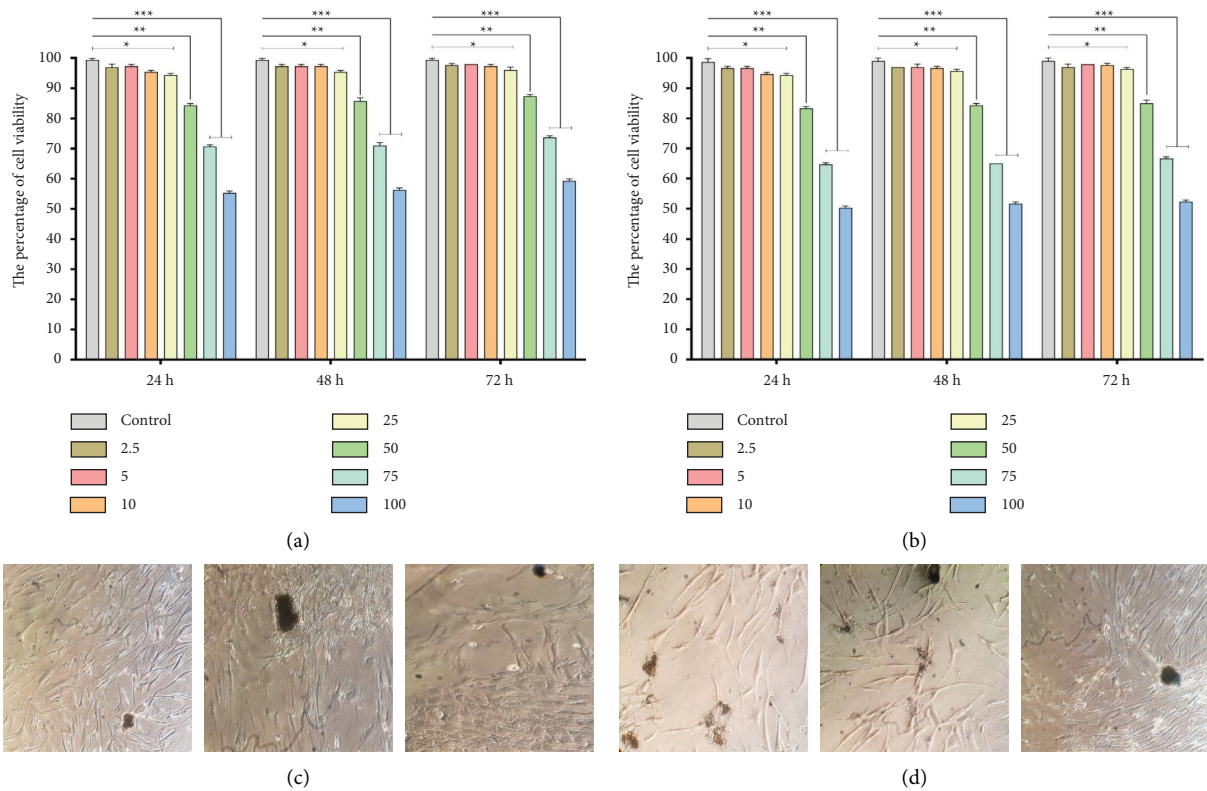


FIGURE 5: Cytotoxicity test of samples 1 and 2: (a) green synthesized CuO NPs from Khalkhal (sample 1), (b) Gillan (sample 2) (CuO NPs concentration: 2.5, 5, 10, 25, 50, 75, and 100 μg/mL and control: cell culture) (* $P < 0.05$), ** $(P < 0.01)$, and *** $(P < 0.001)$), (c) the treated cell culture with CuO NPs sample 1, and (d) sample 2.

4. Discussion

Health risks arise from biofilms containing pathogenic microorganisms. Lactobacillus species can colonize tooth

surfaces due to bacterial adhesion. Along with mechanical plaque removal, natural antimicrobial mouthwashes enhance it. Chlorhexidine mouthwashes promote tooth decay more than herbal mouthwashes [13]. Global public health

TABLE 2: MIC and MBC of green synthesized CuO NPs from Khalkhal (sample 1) and Gillan (sample 2).

Bacteria	Sample 1		Sample 2	
	MIC (mg/ml)	MBC (mg/ml)	MIC (mg/ml)	MBC (mg/ml)
<i>L. acidophilus</i>	0.0024	0.0024	0.0024	0.0024

TABLE 3: The biofilm formation percentages of species treated (10× MBC) with green synthesized CuO NPs from Khalkhal (sample 1), Gillan (sample 2), and chlorhexidine 0.2% (CHX 0.2%).

Bacteria	OD (570 nm)		
	Sample 1	Sample 2	CHX 0.2 (%)
<i>L. acidophilus</i>	6.14%	5.11%	0.76

TABLE 4: The biofilm degradation percentages of species treated (10× MBC) with green synthesized CuO NPs from Khalkhal (sample 1), Gillan (sample 2), and chlorhexidine 0.2% (CHX 0.2%).

Bacteria	OD (570 nm)		
	Sample 1	Sample 2	CHX 0.2 (%)
<i>L. acidophilus</i>	82.29%	79.39%	98.34

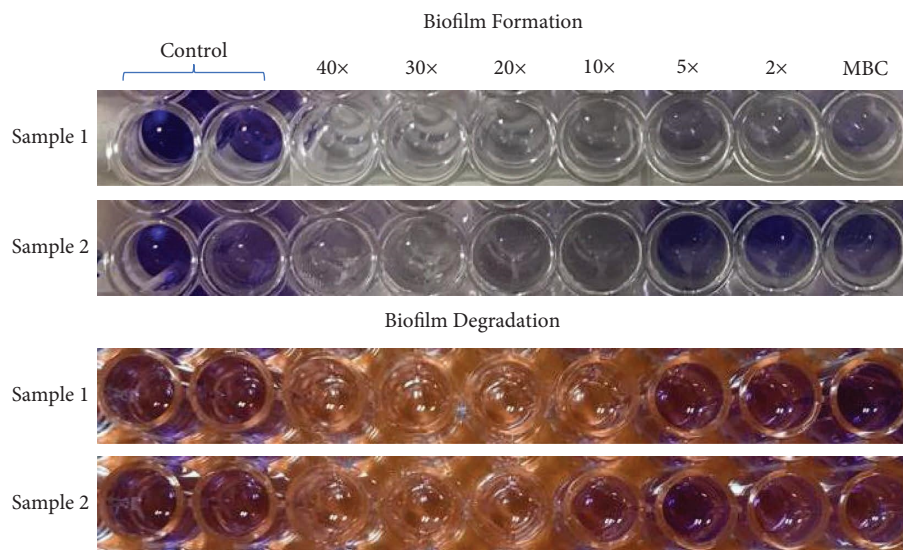


FIGURE 6: The biofilm formation and degradation tests of samples 1 and 2 NPs. Green synthesized CuO NPs from Khalkhal (sample 1) and Gillan (sample 2).

has been affected by AMR in recent years. MDR strains of pathogenic bacteria are becoming more resistant to antibiotics due to the emerging trend of AMR. Recently, metallic nanoscale materials have been used more frequently in nanotechnology. The NPs show promising therapeutic effects due to their unique physicochemical properties [36, 37]. In addition, NPs require a thorough understanding of their physicochemical characteristics and appropriate synthesis methods [36, 38]. A new method for synthesizing metal NPs has been developed by utilizing biological cells' highly structured physical and biosynthetic activities. As nanotechnology continues to improve, it is now used in nearly all biomedical applications, from laboratory to large-

scale manufacturing. In this study, CuO NPs were synthesized using phase-pure, green propolis extract. Due to phenolic compounds, antimicrobial properties are present in natural materials [39]. In Barbosa et al., silver NPs (AgNP-P) were synthesized from Brazilian propolis and studied for their antimicrobial properties. A factorial design was used to optimize the synthesis conditions for smaller particles. UV-visible spectra revealed that AgNP-P was formed in a spherical structure, with maximum absorbance at 412 nm. This new material shows a good size distribution and a low polydispersity index resulting from dynamic light scattering. Silver NPs were found to contain propolis after centrifugation, and microscopy analysis confirmed it. The principal

planes of the metallic silver crystalline structure were identified by X-ray diffraction, while infrared spectroscopy indicated that 22% of the AgNP-P in the sample was reduced to silver. Silver NPs and propolis synergistically demonstrated antimicrobial activity and had significant antimicrobial effects [40].

The CuO NPs were synthesized by Hajizadeh et al. and characterized by FTIR, XRD, and UV-Vis absorption spectra. According to FTIR analysis, propolis extract compounds were found to modify the surface of synthesized NPs. There was a sharp peak at 3422 cm^{-1} in the spectrum of the CuO NPs of the Khalkhal sample. An investigation of UV-Vis spectrophotometry indicates that CuO NPs showed SPR with CuO NPs of the Khalkhal sample at 385 nm. Moreover, CuO NPs of the Gillan sample demonstrated peaks at 243, 292, and 350 nm wavelengths. According to an XRD pattern of the CuO NPs of the Khalkhal sample, the crystallographic planes were 35.74° , 39.04° , and 49.04° and also, 25.54° , 26.69° , 38.79° , and 48.84° were for CuO NPs of Gillan sample [35].

Manikandan et al. report that green-fabricated CuO NPs with a -17.2 mV zeta potential could have more excellent colloidal stability when fabricated from a higher negative charge. NP's catalytic activity is primarily influenced by its surface area, crystal size, and crystallinity. It may be possible for NPs to be highly photocatalytic if the BET value is high, the crystal size is small, and the crystallinity is high. Using propolis increased the rate of photodegradation and specific surface area while decreasing crystal size [41].

According to Moustakas et al., acute CuO NPs exposure caused photosynthetic activity, oxidative stress, and CuO bioaccumulation in seagrasses (*Cymodocea nodosa*). The CuO NPs were characterized with SEM and DLS measurements at 4, 12, 24, 48, and 72 hours (Optimum CuO NPs exposure). In terms of size distribution, CuO NPs synthesized with Pdi 0.35 had an average size of 233 nanometers based on their results [42]. The present study demonstrated that propolis extract could be used to synthesize CuO NPs, but no smaller particles were found. Khalkhal and Gillan propolis extracts were found to interact with CuO NPs in terms of physical interactions.

Green tea (*Camellia sinensis L.*) and lavender (*Lavandula angustifolia*) have been found to synthesize green and pure CuO NPs, respectively. Based on SEM images of lavender-produced samples, it appears that NPs tightly adhered to each other, and lavender was more efficient in generating pure and uniform CuO NPs (50 nm) [43]. A compact distribution of NPs was observed with narrow dispersion. According to the average particle size measurement, NPs were spherical and ranged from 75 to 145 nm for sample 1 (extracted from Khalkhal) and 120 to 155 nm for sample 2 (extracted from Gillan). It has been possible to detect aggregates and NPs of synthetic CuO NPs with spherical shapes on a micrograph.

Veisi et al. studied CuO NPs synthesis with the help of aqueous extracts of *Stachys lavandulifolia* flowers, and they demonstrated that TEM analysis provides morphological information about CuO NPs shapes and dimensions. According to the authors, NPs are synthesized with

moderately good monodispersity, with sizes ranging between 15 and 25 nm without agglomeration [44]. As the surface-to-volume ratio decreases, the particle size decreases inversely, facilitating easy penetration of the cell wall and rapid destruction of microorganisms; Khalkhal and Gillan (Khalkhal and Gillan) propolis extract enhanced the antimicrobial activity of green synthesized CuO NPs.

Botteon et al. (2021) described the biosynthesis of AuNPs and evaluated their structural properties. An SPR band was observed at 535 nm in AuNPs. The Brazilian red propolis (BRP) sample used in the reaction affected the sizes and morphologies. All strains tested showed antimicrobial activity against AuNPdichloromethane and AuNPhexane. In both T24 and PC-3 cells, AuNPs showed dose-dependent cytotoxicity. ANPdichloromethane and AuNPextract were the most cytotoxic. Apoptosis-related mechanisms are also responsible for biogenic nanoparticle cytotoxicity [12]. Rao and colleagues employed the coprecipitation method to stabilize and cap Zinc oxide NPs (2018). NPs (PZnO) were synthesized from P betel. PZnO was tested for its antibacterial activity against dental pathogens using a well-diffusion method. Both tested microbes were inhibited by PZnO at concentrations of as low as $3.25\text{ }\mu\text{g/mL}$, indicating higher antimicrobial activity than DZnO. PZnO and DZnO inhibited cellular growth by 40% using Balb 3T3 mouse fibroblast cell lines [45]. There were no significant cytotoxicity results during the incubation of samples 1 and 2 NPs during the 24, 48, and 72 hours of incubation, which showed that the viability of the samples was approximately more significant than 50%.

NPs synthesized from biosynthetic materials were subjected to MTT assays to assess their impact, and they significantly reduced the survival of cancer cells. NPs synthesized using green methods have been shown to possess antiproliferative properties against cancer cell lines [46, 47]. Silver NPs were green synthesized using leaf extract from *Justicia glauca* by Emmanuel et al. AgNO₃ solution was mainly reduced to AgNPs by water-soluble organics in leaf extracts. TEM images showed that AgNPs were 10–20 nm in diameter. *S. mutans*, *S. aureus*, *L. acidophilus*, and *C. albicans* were used, and the antibacterial and antifungal activities of AgNPs were demonstrated. AgNPs demonstrated MICs between 25 and 75 g/mL [6]. Based on extracts of *A. javanica* leaf, CuO NPs' antibacterial properties were evaluated against *P. aeruginosa*, *E. coli*, *S. aureus*, and *A. baumannii*. There was greater effectiveness of the CuO NPs against *S. aureus*, *P. aeruginosa*, *A. baumannii*, and *E. coli*. According to the sample, *S. aureus* had a maximum inhibition zone of $9 \pm 1\text{ mm}$ in the sample. As a result of the extractions with *A. javanica*, *P. aeruginosa* displayed an even more significant inhibition zone. The pathogens that were most active against CuO NPs were *S. aureus*, *A. baumannii*, *P. aeruginosa*, and *E. coli*, while those with minor activity were *E. coli* and *P. aeruginosa*. It has been demonstrated previously that *S. aureus* was more susceptible to CuO NPs than *E. coli*, based on a comparison between the two samples [48]. There was no difference between samples 1 and 2 in terms of their effect on *L. acidophilus* (0.0024 mg/ml) in the MIC and MBC tests in this study. It was found that the effect

of green synthesized CuO NPs from Khalkhal (sample 1) on biofilm formation was more effective than green synthesized CuO NPs from Gillan (sample 2).

5. Conclusion

The use of nontoxic, cost-effective, ecofriendly, and easy-to-use materials have proven successful and expanded. All samples were tested for cytotoxicity, and it showed that all samples were free of any notable cytotoxicity. In addition, the results showed that the green synthesized CuO NPs from propolis had antibacterial effects against *L. acidophilus*. It can be concluded that green synthesized CuO NPs derived from propolis may be the best candidate for clinical application due to their high antibacterial properties.

Data Availability

The data generated or analyzed during this study are included in this published article.

Conflicts of Interest

The authors declare that they have no conflicts of interest.

Acknowledgments

The authors would like to thank “The Clinical Research Development Unit of Baqiyatallah Hospital for guidance and advice.”

References

- [1] M. Chittrarasu, A. S. Ahamed, and V. Ravi, “Antimicrobial efficacy of green synthesis of silver nanoparticles against cariogenic pathogens - an in vitro study,” *Journal of Pharmacy and BioAllied Sciences*, vol. 13, no. 2, pp. S1188–S1192, 2021.
- [2] P. Abishad, J. Vergis, V. Unni et al., “Green synthesized silver nanoparticles using *Lactobacillus acidophilus* as an antioxidant, antimicrobial, and antibiofilm agent against multi-drug resistant enteroaggregative *Escherichia coli*,” *Probiotics and antimicrobial proteins*, vol. 14, no. 5, pp. 904–914, 2022.
- [3] B. Malaekheh-Nikouei, B. S. Fazly Bazzaz, E. Mirhadi, A. S. Tajani, and B. Khameneh, “The role of nanotechnology in combating biofilm-based antibiotic resistance,” *Journal of Drug Delivery Science and Technology*, vol. 60, Article ID 101880, 2020.
- [4] L. Wang, H. Yue, D. Yang et al., “Metal-free oxidative coupling of aromatic alkenes with thiols leading to (E)-Vinyl sulfones,” *Journal of Organic Chemistry*, vol. 82, no. 13, pp. 6857–6864, 2017.
- [5] X. Y. Wong, A. Sena-Torralba, R. Álvarez-Diduk, K. Muthoosamy, and A. Merkoçi, “Nanomaterials for nanotheranostics: tuning their properties according to disease needs,” *ACS Nano*, vol. 14, no. 3, pp. 2585–2627, 2020.
- [6] R. Emmanuel, S. Palanisamy, S. M. Chen et al., “Antimicrobial efficacy of green synthesized drug blended silver nanoparticles against dental caries and periodontal disease causing microorganisms,” *Materials Science and Engineering: C*, vol. 56, pp. 374–379, 2015.
- [7] M. Yazdani, P. Rostamzadeh, M. Rahbar et al., “The potential application of green-synthesized metal nanoparticles in dentistry: a comprehensive review,” *Bioinorganic Chemistry and Applications*, vol. 2022, Article ID 2311910, 27 pages, 2022.
- [8] M. Yazdani, M. N. Motallaei, E. Tahmasebi et al., “Chemical characterization and cytotoxic/antibacterial effects of nine Iranian propolis extracts on human fibroblast cells and oral bacteria,” *BioMed Research International*, vol. 2022, Article ID 6574997, 14 pages, 2022.
- [9] A. Moghaddam, R. Ranjbar, M. Yazdani et al., “The current antimicrobial and antibiofilm activities of synthetic/herbal/biomaterials in dental application,” *BioMed Research International*, vol. 2022, Article ID 8856025, 26 pages, 2022.
- [10] P. E. F. Barzegar, R. Ranjbar, M. Yazdani et al., “The current natural/chemical materials and innovative technologies in periodontal diseases therapy and regeneration: a narrative review,” *Materials Today Communications*, vol. 2022, Article ID 104099, 32 pages, 2022.
- [11] M. Yazdani, A. Rahmani, E. Tahmasebi, H. Tebyanian, A. Yazdani, and S. A. Mosaddad, “Current and advanced nanomaterials in dentistry as regeneration agents: an update,” *Mini-Reviews in Medicinal Chemistry*, vol. 21, no. 7, pp. 899–918, 2021.
- [12] C. E. A. Botteon, L. B. Silva, G. V. Ccana-Ccapatinta et al., “Biosynthesis and characterization of gold nanoparticles using Brazilian red propolis and evaluation of its antimicrobial and anticancer activities,” *Scientific Reports*, vol. 11, no. 1, p. 1974, 2021.
- [13] M. Yazdani, P. Rostamzadeh, M. Alam et al., “Evaluation of antimicrobial and cytotoxic effects of Echinacea and Arctium extracts and Zataria essential oil,” *AMB Express*, vol. 12, no. 1, p. 75, 2022.
- [14] E. Tafazoli Moghadam, M. Yazdani, M. Alam et al., “Current natural bioactive materials in bone and tooth regeneration in dentistry: a comprehensive overview,” *Mater Res Technol*, vol. 13, pp. 2078–2114, 2021.
- [15] M. N. Motallaei, M. Yazdani, H. Tebyaniyan et al., “Evaluation of cytotoxic and antimicrobial properties of Iranian sea salts: an in vitro study,” *Evidence-based Complementary and Alternative Medicine: eCAM*, vol. 2021, Article ID 8495596, 7 pages, 2021.
- [16] M. N. Motallaei, M. Yazdani, H. Tebyanian et al., “The current strategies in controlling oral diseases by herbal and chemical materials,” *Evidence-based Complementary and Alternative Medicine*, vol. 2021, Article ID 3423001, 22 pages, 2021.
- [17] L. K. Hakim, M. Yazdani, M. Alam et al., “Biocompatible and biomaterials application in drug delivery system in oral cavity,” *Evidence-based Complementary and Alternative Medicine*, vol. 2021, Article ID 9011226, 12 pages, 2021.
- [18] E. Tahmasebi, M. Alam, M. Yazdani et al., “Current biocompatible materials in oral regeneration: a comprehensive overview of composite materials,” *Journal of Materials Research and Technology*, vol. 9, no. 5, pp. 11731–11755, 2020.
- [19] M. C. Zambonino, E. M. Quizhpe, F. E. Jaramillo et al., “Green synthesis of selenium and tellurium nanoparticles: current trends, biological properties and biomedical applications,” *International Journal of Molecular Sciences*, vol. 22, no. 3, p. 989, 2021.
- [20] M. V. Arasu, R. Thirumamagal, M. P. Srinivasan et al., “Green chemical approach towards the synthesis of CeO(2) doped with seashell and its bacterial applications intermediated with fruit extracts,” *Journal of Photochemistry and Photobiology B: Biology*, vol. 173, pp. 50–60, 2017.

- [21] H. Seifi Kafshgari, M. Yazdani, R. Ranjbar et al., "The effect of *Citrullus colocynthis* extracts on *Streptococcus mutans*, *Candida albicans*, normal gingival fibroblast and breast cancer cells," *Journal of Biological Research*, vol. 92, no. 1, p. 8201, 2019.
- [22] H. Kumar, K. Bhardwaj, R. Sharma et al., "Potential usage of edible mushrooms and their residues to retrieve valuable supplies for industrial applications," *Journal of Fungi*, vol. 7, no. 6, p. 427, 2021.
- [23] N. A. Lashgari, N. Momeni Roudsari, D. Khayatan et al., "Ginger and its constituents: role in treatment of inflammatory bowel disease," *BioFactors*, vol. 48, no. 1, pp. 7–21, 2022.
- [24] M. L. Martins, K. L. d F. Leite, E. F. Pacheco-Filho et al., "Efficacy of red propolis hydro-alcoholic extract in controlling *Streptococcus mutans* biofilm build-up and dental enamel demineralization," *Archives of Oral Biology*, vol. 93, pp. 56–65, 2018.
- [25] X. Zhang, Y. Li, X. Luo, and Y. Ding, "Enhancing antibacterial property of porous titanium surfaces with silver nanoparticles coatings via electron-beam evaporation," *Journal of Materials Science: Materials in Medicine*, vol. 33, no. 7, p. 57, 2022.
- [26] M. I. Said, A. A. Othman, and E. M. Abd Elhakeem, "Structural, optical and photocatalytic properties of mesoporous CuO nanoparticles with tunable size and different morphologies," *RSC Advances*, vol. 11, no. 60, pp. 37801–37813, 2021.
- [27] J. Iqbal, A. Andleeb, H. Ashraf et al., "Potential antimicrobial, antidiabetic, catalytic, antioxidant and ROS/RNS inhibitory activities of *Silybum marianum* mediated biosynthesized copper oxide nanoparticles," *RSC Advances*, vol. 12, no. 22, pp. 14069–14083, 2022.
- [28] A. Monks, D. Scudiero, P. Skehan et al., "Feasibility of a high-flux anticancer drug screen using a diverse panel of cultured human tumor cell lines," *JNCI Journal of the National Cancer Institute*, vol. 83, no. 11, pp. 757–766, 1991.
- [29] M. Yazdani, H. Tabesh, B. Houshmand et al., "Fabrication and properties of β TCP/Zelite/Gelatin scaffold as developed scaffold in bone regeneration: in vitro and in vivo studies," *Biocybernetics and Biomedical Engineering*, vol. 40, no. 4, pp. 1626–1637, 2020.
- [30] S. A. Mosaddad, M. Yazdani, H. Tebyanian et al., "Fabrication and properties of developed collagen/strontium-doped Bioglass scaffolds for bone tissue engineering," *Journal of Materials Research and Technology*, vol. 9, no. 6, pp. 14799–14817, 2020.
- [31] R. S. Soufdoost, M. Yazdani, E. Tahmasebi et al., "In vitro and in vivo evaluation of novel Tadalafil/ β -TCP/Collagen scaffold for bone regeneration: a rabbit critical-size calvarial defect study," *Biocybernetics and Biomedical Engineering*, vol. 39, no. 3, pp. 789–796, 2019.
- [32] S. K. Verma, E. Jha, P. K. Panda et al., "Mechanistic insight into size-dependent enhanced cytotoxicity of industrial antibacterial titanium oxide nanoparticles on colon cells because of reactive oxygen species quenching and neutral lipid alteration," *ACS Omega*, vol. 3, no. 1, pp. 1244–1262, 2018.
- [33] M. M. Tarpay, D. F. Welch, and M. I. Marks, "Antimicrobial susceptibility testing of *Streptococcus pneumoniae* by microbroth dilution," *Antimicrobial Agents and Chemotherapy*, vol. 18, no. 4, pp. 579–581, 1980.
- [34] J. J. Veloz, M. Alvear, and L. A. Salazar, "Evaluation of alternative methods to assess the biological properties of propolis on metabolic activity and biofilm formation in *Streptococcus mutans*," *Evidence-based Complementary and Alternative Medicine: eCAM*, vol. 2019, Article ID 1524195, 8 pages, 2019.
- [35] Y. S. Hajizadeh, N. Harzandi, E. Babapour, M. Yazdani, and R. Ranjbar, "Green synthesis and characterization of copper nanoparticles using Iranian propolis extracts," *Advances in Materials Science and Engineering*, vol. 2022, Article ID 8100440, 9 pages, 2022.
- [36] M. Kawish, F. Ullah, H. S. Ali et al., "Chapter 10 - bactericidal potentials of silver nanoparticles: novel aspects against multidrug resistance bacteria," in *Metal Nanoparticles for Drug Delivery and Diagnostic Applications*, M. R. Shah, M. Imran, and S. Ullah, Eds., pp. 175–188, Elsevier, Amsterdam, Netherlands, 2020.
- [37] T. Lee, S. Y. Park, H. Jang et al., "Fabrication of electrochemical biosensor consisted of multi-functional DNA structure/porous Au nanoparticle for avian influenza virus (H5N1) in chicken serum," *Materials Science and Engineering: C*, vol. 99, pp. 511–519, 2019.
- [38] A.-C. Burduşel, O. Gherasim, A. M. Grumezescu, L. Mogoantă, A. Ficai, and E. Andronescu, "Biomedical applications of silver nanoparticles: an up-to-date overview," *Nanomaterials*, vol. 8, no. 9, p. 681, 2018.
- [39] M. S. Almuhayawi, "Propolis as a novel antibacterial agent," *Saudi Journal of Biological Sciences*, vol. 27, no. 11, pp. 3079–3086, 2020.
- [40] V. T. Barbosa, J. K. C. Souza, V. Alvino et al., "Biogenic synthesis of silver nanoparticles using Brazilian propolis," *Biotechnology Progress*, vol. 35, no. 6, p. e2888, 2019.
- [41] D. B. Manikandan, M. Arumugam, S. Veeran et al., "Biofabrication of ecofriendly copper oxide nanoparticles using *Ocimum americanum* aqueous leaf extract: analysis of in vitro antibacterial, anticancer, and photocatalytic activities," *Environmental Science and Pollution Research*, vol. 28, no. 26, pp. 33927–33941, 2021.
- [42] M. Moustakas, P. Malea, K. Haritonidou, and I. Spirdouli, "Copper bioaccumulation, photosystem II functioning, and oxidative stress in the seagrass *Cymodocea nodosa* exposed to copper oxide nanoparticles," *Environmental Science and Pollution Research*, vol. 24, no. 19, pp. 16007–16018, 2017.
- [43] I. Khaldari, M. R. Naghavi, and E. Motamedi, "Synthesis of green and pure copper oxide nanoparticles using two plant resources via solid-state route and their phytotoxicity assessment," *RSC Advances*, vol. 11, no. 6, pp. 3346–3353, 2021.
- [44] H. Veisi, B. Karmakar, T. Tamoradi, S. Hemmati, M. Hekmati, and M. Hamelian, "Biosynthesis of CuO nanoparticles using aqueous extract of herbal tea (*Stachys Lavandulifolia*) flowers and evaluation of its catalytic activity," *Scientific Reports*, vol. 11, no. 1, p. 1983, 2021.
- [45] S. P. Rao, K. Byrappa, N. Keerthiraj, J. Chatterjee, and M. S. Mustak, "Phyto-fabrication of ZnO nanoparticles using piper betel aqueous extract and evaluation of its applicability in dentistry," *Pharmaceutical Nanotechnology*, vol. 6, no. 3, pp. 201–208, 2018.
- [46] A. Chatterjee, D. Nishanthini, N. Sandhiya, and J. Abraham, "Biosynthesis of titanium dioxide nanoparticles using *Vigna*

- radiata," *Asian Journal of Pharmaceutical and Clinical Research*, pp. 85–88, 2016.
- [47] R. D. A. Jalil, "Antagonistic effect between Citrullus colocynthis extract and TiO₂ nanoparticles in anticancer combination therapy," *Iraqi Journal of Cancer and Medical Genetics*, vol. 9, no. 2, 2016.
- [48] S. Gunalan, R. Sivaraj, and R. Venkatesh, "Aloe barbadensis Miller mediated green synthesis of mono-disperse copper oxide nanoparticles: optical properties," *Spectrochimica Acta Part A: Molecular and Biomolecular Spectroscopy*, vol. 97, pp. 1140–1144, 2012.

Research Article

The Feasibility of Choosing D4 Embryo Transfer—Analysis of Nanomaterials Affecting the Outcome of Frozen-Thaw Embryo Transfer

Chang Tan, Xiliang Wang, Lishuang Luo, Jinyan Zhang, Pengshu Zou, Wei Wei, and Yuexin Yu 

Department of Reproductive Medicine, General Hospital of Northern Theater Command, Shenyang 110003, Liaoning, China

Correspondence should be addressed to Yuexin Yu; yuyuexin@sjjqzzyy.org.cn

Received 11 August 2022; Revised 21 September 2022; Accepted 26 September 2022; Published 10 October 2022

Academic Editor: Fernanda Tonelli

Copyright © 2022 Chang Tan et al. This is an open access article distributed under the Creative Commons Attribution License, which permits unrestricted use, distribution, and reproduction in any medium, provided the original work is properly cited.

FET is to resuscitate the endometrium and transfer the embryo into the uterus after the endometrium is ready. The quality of transferred embryos is an important factor affecting the outcome of assisted reproductive technology. This paper aims to explore the feasibility of D4 frozen-thaw embryo transfer and analysis of related factors affecting the outcome of freeze-thaw embryo transfer. A retrospective analysis of the clinical data of 2925 patients who received frozen-thaw embryo transfer (FET) in the Department of Reproductive Medicine, General Hospital of Northern Theater Command from January 1, 2017 to July 31, 2019. Including the woman's age, body mass index (BMI), endometrial thickness on the day of transplantation, number of embryos to be transferred, and type of embryos to be transferred. A single factor, multivariate logistic regression and nomogram were used to analyze the influence of different factors on the clinical outcome of FET. Nanomedicines and related nanomedicines are rapidly developing and establishing their importance in embryo transfer. This paper uses nanomaterials to explore the feasibility of D4 frozen-thawed embryo transfer. The woman's age, endometrial thickness on the day of transplantation, BMI, the number of embryos transferred, and the type of embryos transferred all affect the outcome of FET. The pregnancy rate of the D5 and D4 transplantation groups was, respectively, higher than that of the D3 transplantation group, with statistically significant differences. In the FET cycle, the age of the woman, endometrial thickness on the day of transplantation, the number of embryos transferred, and the type of embryos transferred are all independent factors influencing the outcome of FET. D5 blastocyst is the easiest to get pregnant, and that has the best clinical outcome which is better than the D6 blastocyst group; D4 morula and D5 blastocyst FET have little difference in clinical pregnancy outcomes, but both of them are significantly better than D3 cell embryos, so D4 morula can be considered for transplantation in the FET cycle. In conclusion, whether it is a patient who has failed the fresh cycle transplantation or the whole embryo freezing cycle whose transplantation is canceled due to high hormone levels on the transplantation day, FET is required.

1. Introduction

With the rapid development of assisted reproductive technology, the technology of embryo cryopreservation and embryo culture technique in vitro are becoming more and more perfect and stable, and they are widely used by reproductive centers around the world. On the one hand, frozen-thawed embryo transfer (FET) can reasonably control the number of embryos transferred and avoid the occurrence of multiple pregnancies. On the other hand, FET

can not only reduce the occurrence of ovarian hyperstimulation syndrome when the embryo is synchronized with the endometrial “implantation window,” but it can also increase the embryo implantation rate and the cumulative pregnancy rate of a single oocyte retrieval cycle, and reduce the patients' treatment costs [1, 2]. FET has been widely used clinically. Many factors affect the clinical outcome of FET, and embryo quality is one of them. Many research results suggest that blastocyst should be thawed first in the cycle of FET, but in actual clinical work, due to individual differences in patients,

the success rate of each blastocyst transfer cannot be guaranteed. There are many studies on the influence of the endometrial preparation program on FET pregnancy, but most studies believe that it has no effect [3, 4]. Studies have reported that under natural physiological conditions, early embryos develop in the fallopian tube and do not enter the uterine cavity until they are close to the blastocyst stage [5]. Blastocyst transfer is more in line with natural physiological phenomena, so blastocyst transfer can improve the clinical pregnancy rate and embryo implantation rate [6–8]. There have always been different research reports on the developmental potential of blastocysts at different times. Some scholars believe that there is no significant difference in clinical pregnancy rates after transplantation of D5 and D6 freeze-thawed blastocysts [9, 10]. Studies have also shown that the clinical pregnancy rate of D5 freeze-thawed blastocyst transplantation is significantly higher than that of D6 [11].

Therefore, how to choose the most suitable embryo for transplantation to increase the pregnancy rate while minimizing the number of the embryo and the multiple pregnancy rate in the cycle of FET is an urgent problem to be solved in clinical work. This article retrospectively analyzes the clinical outcomes of 2925 FET cycles from January 2017 to July 2019 and further compares frozen-thawed embryos at different times and other related factors that affect the outcome of FET, providing a useful reference for the selection of embryos for FET cycles.

2. Materials and Methods

2.1. Research Object. The data of patients who underwent FET in our department from 2017.01 to 2019.07 were collected, and a total of 2925 cycles were included for retrospective analysis. Inclusion criteria are as follows: (1) Age <45 years old (2) Number of embryo transfers ≤ 2 , excluding (1) patients with previous ovarian surgery history, genital malformations, endometriosis, submucosal fibroids and intrauterine adhesions, hydrosalpinx and other factors that may affect embryo implantation. (2) Chromosomal abnormality in either partner (3) cycles of preimplantation genetic testing (PGT). The endometrium preparation of all patients in this study adopted hormone replacement therapy. The study was reviewed and approved by the medical Ethics Committee of our hospital, and the freeze-thaw embryo transfer was performed with the full informed consent of the patients. Collecting patients data, patients are divided into ≤ 35 years old group, >35 years old group by age; that are divided into ≤ 0.8 cm group, $0.81\sim 1.0$ cm group, and >1.0 cm group according to endometrial thickness on the embryo transfer day; and divided into ≤ 18.5 group, $18.6\sim 23.9$ group, $24\sim 26.9$ group, $27\sim 29.9$ group, and >30 groups by BMI; the number of embryos transferred is divided into 1 embryo transfer group and 2 embryos group; according to the morphology of embryo transfer, they are divided into D3 frozen-thawed embryo transfer group, D4 frozen-thawed embryo transfer group, D5 frozen-thawed embryo transfer group, and D6 frozen-thawed embryo transfer group.

2.2. Research Methods. Among assisted reproductive technology, such as perform in vitro fertilization (IVF) or intracytoplasmic sperm injection (ICSI). The first day after fertilization, embryologists judge fertilization by the presence of double pronucleus, and record the number of blastomeres and embryo grading according to the Peter cleavage scoring system. They select D3 high-quality cleavage embryos to freeze, and the remaining embryos continue to be cultured after the patients' informed consent. D4 embryo develops into morula embryos. If the D5 or D6 embryo develops into blastocyst that formation would be recorded, using Gardner scoring system scores blastocysts [12].

2.2.1. Embryo Culture and Score. The standard of embryo freezing in this laboratory is: on the D3, we select high-quality cleavage embryos that divide into 7–9 cells, with uniform blastomeres and fragment rates less than 10% for freezing [13]. If the embryo developed into a morula on D4, that would be frozen. The blastocysts would be frozen with a score of 3BC or above on D5. If D5 does not develop blastocysts that meet the standard, continue to culture until day 7, during which embryos that meet the standard will be frozen again. When the patient has no blastocysts that meet the standards of 3BC or 3CB, the secondary embryos will be frozen after being informed and signed informed consent.

2.2.2. Cryopreservation. We adopt vitrification freezing technology, before freezing, laser drilling is used to artificially shrink the blastocyst to release the liquid in the blastocyst cavity. The resuscitated embryos are incubated with laser. For the blastocyst and morula, the zona pellucida away from the inner cell mass is punched through, and the zona pellucida of cleavage embryo is thinned. The resuscitated embryos are transferred to the pre-equilibrated culture medium the previous day, and placed in the incubator for culture. They are observed before transplantation, the survival of embryos is determined according to whether the blastocyst cavity, morulae are re-expanded, and the number of cells survived by cleavage embryos after thawing [14].

2.2.3. Endometrial Preparation. Compared with fresh cycle transplantation, the FET cycle endometrial and embryonic development are more synchronized. There are many studies on the influence of the endometrial preparation program on FET pregnancy, but most studies believe that it has no effect [3, 4]. All patients enrolled in this study used a hormone replacement cycle: starting from the 3rd to 5th day of the menstrual cycle, oral estradiol valerate (Progynat, Bayer, Germany) was administered 4–6 mg daily, and the thickness of endometrium was monitored by ultrasound after 7 days. Thickness and hormone levels. Adjust the dosage of estradiol valerate in time. When the endometrial thickness needs to reach at least 0.6 cm, an intramuscular injection of 40–60 mg/d of progesterone is injected to support the corpus luteum. Blastocyst transplantation was performed on the 5th

or 6th day after the ketone injection. D5 or D6 blastocysts were selected for resuscitation and transplantation.

2.2.4. Observation Indicators and Evaluation Criteria. Test blood human chorionic gonadotropin (β -HCG) on the 14th day after embryo transfer. If it is positive and 4 to 5 weeks after transplantation, a vaginal B-ultrasound examination is performed. The gestational sac and heart tube pulsation in the uterus are clinically pregnant, and the corpus luteum support is continued until 10 to 12 weeks of pregnancy, and the follow-up is to live birth.

2.3. Statistical Methods. Statistical analysis was performed using SPSS 25.0 software. Continuous variable data is expressed in the form of mean \pm standard deviation $x \pm s$, independent samples t -test is used, and t' test is used when the variance is not homogeneous; categorical variable data is expressed in the form of n (%), and the nonparametric chi-square test is used for group analysis. If the frequency is less than 5 and greater than or equal to 1, the continuous correction chi-square test is used; logistic regression is used for multivariate regression analysis; R language (4.1.1) is used to draw a nomogram. The analysis results were considered statistically significant at $P \leq 0.05$.

3. Results

3.1. Basic Data of Patients during the Frozen-Thaw Embryo Transfer Cycle. The basic clinical data of 2925 patients were collected, with an average age of 33.08 years, an average endometrial thickness of 0.98 cm on the day of transfer, and an average BMI of 23.44. The specific distribution of the number of transferred embryos and the types of transferred embryos is shown in Table 1.

3.2. Analysis of Single Factors Affecting the Pregnancy Outcome of Frozen-Thaw Embryo Transfer Cycle. Univariate analysis of factors that may affect the outcome of FET in patients showed that the woman's age, endometrial thickness, BMI, number of embryos transferred, and embryos on the day of transfer all affected the clinical outcome of FET, and the differences were statistically significant ($P < 0.05$), see Table 2 for details.

3.3. Analysis of Multiple Factors Affecting the Pregnancy Outcome of Frozen-Thaw Embryo Transfer Cycle. Multivariate logistic regression analysis showed (Hosmer-Lemeshaw test $P = 0.897$), the woman's age, endometrial thickness on the day of transfer, BMI, and the embryo on the day of transfer were the influencing factors of pregnancy in the FET cycle; Hosmer-Lemeshaw test ($P = 0.505$). Among them, the clinical outcome of FET of D4 frozen-thawed embryos was better than that of D3 frozen-thawed embryos, and the difference was statistically significant ($P < 0.05$), see Table 3 for details.

3.4. Multivariate Analysis of Transferring D4 Frozen-Thawed Embryos and D5 Frozen-Thawed Embryos as Controls. Using D4 frozen-thawed embryos as the control standard, multivariate logistic regression analysis showed that in the FET cycle, the clinical outcome of D4 frozen-thawed embryos was better than that of D3 frozen-thawed embryos, and the difference was statistically significant ($P < 0.05$), but D4 frozen-thawed embryos had a statistically significant difference ($P < 0.05$). There was no significant difference in the outcome of frozen-thawed embryos with D5 and D6 ($P > 0.05$), see Table 4 for details.

Taking D5 frozen-thawed embryos as the control standard, multivariate logistic regression analysis showed that in the FET cycle, the clinical outcome of D5 frozen-thawed embryos was better than that of D6 and D3 frozen-thawed embryos, and the difference was statistically significant ($P < 0.05$). There was no significant difference in the outcomes of thawed embryos and D4 frozen-thawed embryos ($P > 0.05$), see Table 5 for details.

3.5. Nomograms of Factors Influencing the Outcome of Frozen-Thaw Embryo Transfer Cycle. The nomogram (C-Index = 0.628) intuitively shows the correlation between the woman's age, endometrial thickness, body mass index BMI, the number of embryos transferred and the embryos on the first day of transfer and other factors with FET pregnancy, among which age is less than or equal to 35 age, endometrial thickness on the day of transfer > 1.0 cm, BMI greater than or equal to 27 and less than or equal to 29.9, and it is relatively easier to get pregnant after transferring 2 embryos, D5 frozen-thawed embryos have the best correlation with pregnancy, followed by D4 frozen-thawed embryos, and D3 frozen-thawed embryos. Embryo pregnancy had the worst correlation and was relatively least fertile. See Figure 1 for details.

4. Discussion

FET is to resuscitate the endometrium and transfer the embryo into the uterus after the endometrium is ready, so that the endometrium and embryo development tend to be synchronized, the time interval is shortened between further development and implantation after embryo transfer, and the occurrence of complications such as ectopic pregnancy is reduced [15, 16].

As we all know, the quality of transferred embryos is an important factor affecting the outcome of assisted reproductive technology. The study in this article shows that D5 freeze-thawed blastocysts are the most likely to become pregnant in the FET cycle, and the clinical outcome is significantly better than D6 freeze-thawed blastocysts and D3 freeze-thawed blastocysts. The difference is statistically significant, which confirms the second point of view. The reason may be that the development of D6 blastocysts lags one day to form blastocysts. Under the condition that the embryos are recovered without damage, it may be that their developmental speed affects their developmental potential and embryo quality.

TABLE 1: Basic data of patients during the frozen-thaw embryo transfer cycle.

	N (%)	$\bar{x} \pm s$
Age	2925	33.08 ± 4.14
≤35	2154 (73.6)	31.20 ± 2.83
>35	771 (26.4)	38.34 ± 2.25
Endometrial thickness (cm)	2925	0.98 ± 0.21
≤0.8	688 (23.5)	0.72 ± 0.078
0.81~1.0	1247 (42.6)	0.94 ± 0.061
>1.0	990 (33.8)	1.21 ± 0.13
BMI (kg/m ²)	2925	23.44 ± 3.70
≤18.5	175 (5.9%)	17.75 ± 0.83
18.6~23.9	1573 (53.7%)	21.32 ± 1.46
24~26.9	669 (22.8%)	25.29 ± 0.83
27~29.9	331 (11.3%)	28.18 ± 0.82
>30	177 (6.0%)	31.99 ± 1.80
Number of embryos transferred		
1	726 (24.8)	
2	2199 (75.1)	
Day of embryo transferred		
D3	1234 (42.1)	
D4	53 (1.8)	
D5	725 (24.7)	
D6	913 (31.2)	

TABLE 2: Analysis of single factors affecting the pregnancy outcome of frozen-thaw embryo transfer cycle.

	No pregnancy	Pregnancy	<i>t/x</i> ²	<i>P</i>
Age				
$\bar{x} \pm s$	33.80 ± 4.35	32.50 ± 3.86	8.48	<i>P</i> < 0.001
≤35	890 (67.58)	1264 (78.61)	45.37	<i>P</i> < 0.001
>35	427 (32.42)	344 (21.39)		
Endometrial thickness (cm)				
$\bar{x} \pm s$	0.96 ± 0.22	0.93 ± 0.2	-4.80	<i>P</i> < 0.001
≤0.8	372 (28.25)	316 (19.65)		
0.81~1.0	543 (41.23)	704 (43.78)	31.65	<i>P</i> < 0.001
>1.0	402 (30.52)	588 (36.57)		
BMI (kg/m ²)				
$\bar{x} \pm s$	23.22 ± 3.61	23.61 ± 3.76	-2.83	<i>P</i> = 0.005
≤18.5	84 (6.38)	91 (5.7)		
18.6~23.9	744 (56.49)	829 (51.55)		
24~26.9	282 (21.40)	387 (24.1)	10.18	<i>P</i> = 0.037
27~29.9	132 (10.00)	199 (12.4)		
>30	75 (5.70)	102 (6.3)		
Number of embryos transferred				
1	369 (28.02)	357 (22.20)	13.13	<i>P</i> < 0.001
2	948 (71.98)	1251 (77.80)		
Day of embryo transferred				
D3	616 (46.77)	618 (38.43)		
D4	19 (1.44)	34 (2.11)		
D5	254 (19.29)	471 (29.29)	44.25	<i>P</i> < 0.001
D6	428 (32.50)	485 (30.16)		

There are few studies on D4 freeze-thaw mulberry embryo transfer. Embryo development is a “survival of the fittest” selection process. Fertilized eggs gradually cleavage and develop into cellular embryos, morulae, and blastocysts. The morula is an embryo morphology between the cellular embryo and the blastocyst. The embryonic cells at the morula stage are in a dense or semidense state. Some cells that develop faster will also form early blastocysts, and the

cells are tightly connected to form a network. The structure, which constitutes the embryonic skeleton, has good resistance to some drastic changes in the mother’s body, avoids adverse reactions such as miscarriage, and thus increases the pregnancy rate [17]. Studies have shown that even high-quality embryos at the cleavage stage maybe 60% aneuploid, and the aneuploidy rate of embryos that develop into morula and blastocysts can be reduced to about 30% [18]. On the one

TABLE 3: Analysis of multiple factors affecting the pregnancy outcome of frozen-thaw embryo transfer cycle.

	OR (95% CI)	<i>P</i>
Age		<i>P</i> < 0.001
≤35		
>35	0.64 (0.54–0.76)	<i>P</i> < 0.001
Endometrial thickness (cm)		<i>P</i> < 0.001
≤0.8		
0.81~1.0	1.56 (1.28–1.89)	<i>P</i> < 0.001
>1.0	1.74 (1.42–2.13)	<i>P</i> < 0.001
BMI (kg/m ²)		<i>P</i> = 0.74
≤18.5		
18.6~23.9	1.03 (0.75–1.42)	<i>P</i> = 0.852
24~26.9	1.29 (0.91–1.81)	<i>P</i> = 0.151
27~29.9	1.33 (0.91–1.94)	<i>P</i> = 0.143
>30	1.23 (0.80–1.89)	<i>P</i> = 0.350
Number of embryos transferred		<i>P</i> < 0.001
1		
2	1.76 (1.46–2.14)	<i>P</i> < 0.001
Day of embryo transferred		
D3		
D4	1.81 (1.01–3.25)	<i>P</i> = 0.045
D5	2.41 (1.95–2.98)	<i>P</i> < 0.001
D6	1.36 (1.13–1.63)	<i>P</i> = 0.001

TABLE 4: Multivariate analysis of frozen-thawed embryo on Day 4 of transplantation as control.

	OR (95% CI)	<i>P</i>
Day of embryo transferred		<i>P</i> < 0.001
D4		
D3	0.55 (0.31–0.99)	<i>P</i> = 0.045
D5	1.33 (0.73–2.41)	<i>P</i> = 0.358
D6	0.75 (0.42–1.35)	<i>P</i> = 0.331

TABLE 5: Multivariate analysis of frozen-thawed embryo on Day 5 of transplantation as control.

	OR (95% CI)	<i>P</i>
Day of embryo transferred		<i>P</i> < 0.001
D5		
D3	0.42 (0.34–0.51)	<i>P</i> < 0.001
D4	0.76 (0.42–1.37)	<i>P</i> = 0.358
D6	0.56 (0.46–0.69)	<i>P</i> < 0.001

hand, mulberry embryos are developed from cleavage stage embryos with good developmental potential. Embryo culture is a natural selection process for the survival of the fittest. Mulberry embryos are the elimination of developmentally retarded and unfused embryos and form semifusion or fusion. Potential embryo. On the other hand, morula freezing is better than blastocyst freezing. Blastocyst freezing requires artificial shrinkage to remove a large amount of water in the blastocyst cavity. It is easy to form ice

crystals and cause embryo damage, and insufficient dehydration affects the thawing effect [19–23], artificial shrinkage also increases embryo manipulation and in vitro exposure time, which may affect embryo safety. In addition, blastocyst culture requires embryos to be cultured for 5–6 days, which prolongs the exposure time of embryos in vitro. Cell quality and culture environment may affect the development process of embryos, and even affect the formation of blastocysts, resulting in no embryos available. Risk [24].

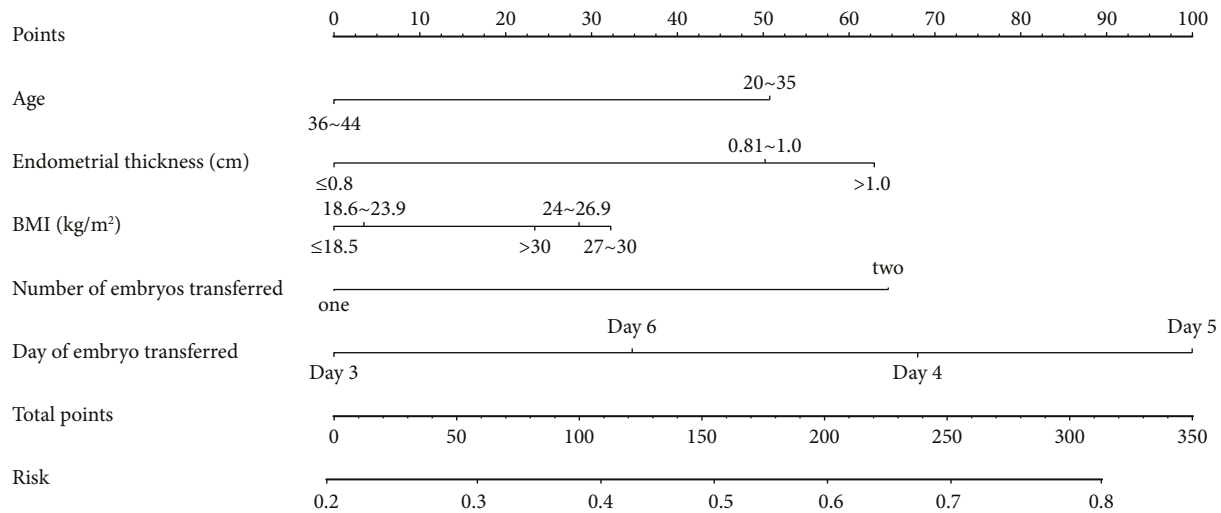


FIGURE 1: Nomograms of factors influencing the outcome of frozen-thaw embryo transfer cycle.

5. Conclusion

To sum up, whether it is a patient who has failed the fresh cycle transplantation or the whole embryo freezing cycle whose transplantation is canceled due to high hormone levels on the transplantation day, FET is required. In the FET cycle, the patient's age, BMI, and embryo development should be fully considered. According to the actual conditions and blastocyst formation, the transplantation plan is tailored for each patient, the appropriate endometrial thickness is adjusted, and the embryos with good development potential are selected for transfer. In the case of patients with more blastocysts, it is recommended to give priority to the recovery of D5 freeze-thawed blastocysts.

The results of this study show that the FET outcome of D5 freeze-thawed blastocysts is the most relevant to pregnancy; if D5 does not form blastocysts, D6 blastocysts can be selected; but if the patient's blastocyst quality is poor or there is no blastocyst formation or the experience of blastocyst transfer failure, D4 freeze-thawed morulae can be considered for FET; this study found that D4 freeze-thaw mulberry embryos and D5 freeze-thawed blastocysts have a similar pregnancy probability. There is no significant difference in clinical outcome, and it is significantly better than D3 freeze-thaw cleavage embryo. Freezing and thawing mulberry embryos for FET is a viable option.

However, there are few studies on D4 freeze-thaw mulberry embryo transfer. And the data are limited in our study. In the future work, we need to collect more data to obtain more scientific results. If some patients have special conditions or have no transplantable D5 blastocysts, using D4 morula for FET is also a new and feasible option, which not only increases FETs. The flexibility of FET, and provides a new idea for the selection of FET embryos.

Data Availability

The datasets used and/or analyzed during the current study are available from the corresponding author upon reasonable request.

Conflicts of Interest

The authors declare no potential conflicts of interest with the respect to the research, authorship, and/or publication of this article.

References

- [1] X. Wang, J. R. Zhen, and Z. Y. Sun, "Effect of cryopreservation time of blastocysts on the clinical outcome of resuscitation and transplantation," *Journal of Reproductive Medicine*, vol. 25, pp. 389–394, 2017.
- [2] Q. R. Liu, Q. Y. Huang, and L. S. Chi, "Effect of vitrification on the outcome of embryo transfer in freeze-thaw cleavage," *International Medical and Health Guide*, vol. 20, no. 23, pp. 3531–3534, 2014.
- [3] K. Hancke, S. More, R. Kreienberg, and J. M. Weiss, "Patients undergoing frozen-thawed embryo transfer have similar live birth rates in spontaneous and artificial cycles," *Journal of Assisted Reproduction and Genetics*, vol. 29, no. 5, pp. 403–407, 2012.
- [4] Y. F. Li, G. J. Zhu, and H. W. Zhang, "Comparison of three methods of preparing endometrium for frozen-thawed embryo transfer," *Chinese Journal of Reproduction and Contraception*, vol. 29, no. 2, pp. 113–116, 2009.
- [5] G. Q. Hao, R. Li, and L. Geng, "Analysis of clinical outcome of embryo transfer and blastocyst transfer," *Chinese Journal of Human Sexuality*, vol. 25, no. 3, pp. 113–116, 2016.
- [6] M. R. Thomas, A. E. Sparks, G. L. Ryan, and B. J. Van Voorhis, "Clinical predictors of human blastocyst formation and

- pregnancy after extended embryo culture and transfer,” *Fertility and Sterility*, vol. 94, no. 2, pp. 543–548, 2010.
- [7] G. Saki, F. Rahim, and L. Moradi, “The study of developmental capacity of vitrified mouse blastocysts in different straws after transfer to mouse pseudo pregnant,” *Pakistan Journal of Biological Sciences*, vol. 11, no. 14, pp. 1809–1814, 2008.
- [8] S. Goto, T. Kadowaki, S. Tanaka, H. Hashimoto, S. Koikeguchi, and M. Shiotani, “Prediction of pregnancy rate by blastocyst morphological score and age, based on 1, 488 single frozen-thawed blastocyst transfer cycles, based on 1488 single frozen-thawed blastocyst transfer cycles,” *Fertility and Sterility*, vol. 95, no. 3, pp. 948–952, 2011.
- [9] Y. N. Hu, T. Ding, and Y. Zhao, “Analysis of the outcome of blastocyst transfer on D5 and D6 Days of fresh cycle of ultralong plan,” *Jiangxi Medical Journal*, vol. 52, no. 4, pp. 335–337, 2017.
- [10] T. El-Toukhy, E. Wharf, R. Walavalkar et al., “Delayed blastocyst development does not influence the outcome of frozen-thawed transfer cycles,” *BJOG*, vol. 118, no. 13, pp. 1551–1556, 2011.
- [11] S. K. Sunkara, A. Siozos, V. N. Bolton, Y. Khalaf, P. R. Braude, and T. El-Toukhy, “The influence of delayed blastocyst formation on the outcome of frozen-thawed blastocyst transfer: a systematic review and meta-analysis: a systematic review and meta-analysis,” *Human Reproduction*, vol. 25, no. 8, pp. 1906–1915, 2010.
- [12] D. K. Gardner, M. Lane, J. Stevens, T. Schlenker, and W. B. Schoolcraft, “Blastocyst score affects implantation and Pregnancy outcome: towards a single blastocyst transfer,” *Fertility and Sterility*, vol. 73, pp. 1155–1158, 2000.
- [13] J. Zhang, “Effect of the number of high-quality embryos transferred on clinical pregnancy rate and multiple pregnancy rate,” *Journal of Reproductive Medicine*, vol. 6, no. 17, pp. 183–186, 2008.
- [14] S. Goto, T. Kadowaki, S. Tanaka, H. Hashimoto, S. Koikeguchi, and M. Shiotani, “Prediction of pregnancy rate by blastocyst morphological score and age, based on 1,488 single frozen-thawed blastocyst transfer cycles,” *Fertility and Sterility*, vol. 95, pp. 948–952, 2011.
- [15] Y. R. Kuai, S. Wang, and K. Zhang, “Analysis of influencing factors of pregnancy outcome in 1008 frozen embryo transfer cycles,” *Chinese Journal of Human Sexuality*, vol. 25, no. 3, pp. 113–116, 2016.
- [16] Q. F. Yu and X. L. Jia, “Comparison of the clinical outcomes of single blastocyst transfer, double blastocyst and double cleavage embryo transfer during resuscitation cycle,” *China Modern Medicine*, vol. 24, no. 26, pp. 90–92, 2017.
- [17] Z. W. Zhao, X. H. Bai, and R. Lv, “Logistic regression analysis of influencing factors of embryo implantation in in vitro fertilization-embryo transfer,” *Chinese Journal of Family Planning*, vol. 21, pp. 681–684, 2013.
- [18] J. Tao, R. Tamis, K. Fink, B. Williams, T. Nelson-White, and R. Craig, “The neglected morula/compact stage embryo transfer,” *Human Reproduction*, vol. 17, no. 6, pp. 1513–1518, 2002.
- [19] P. Vanderzwalmen, G. Bertin, C. Debauche et al., “Births after vitrification at morula and blastocyst stages: effect of artificial reduction of the blastocoelic cavity before vitrification,” *Human Reproduction*, vol. 17, no. 3, pp. 744–751, 2002.
- [20] T. Mukaida, S. Nakamura, T. Tomiyama et al., “Vitrification of human blastocysts using cryoloops: clinical outcome of 223 cycles,” *Human Reproduction*, vol. 18, no. 2, pp. 384–391, 2003.
- [21] T. Mukaida, C. Oka, T. Goto, and K. Takahashi, “Artificial shrinkage of blastocoeles using either a micro-needle or a laser pulse prior to the cooling steps of vitrification improves survival rate and pregnancy outcome of vitrified human blastocysts,” *Human Reproduction*, vol. 21, no. 12, pp. 3246–3252, 2006.
- [22] N. Mesut, M. Bahceci, H. N. Ciray, A. Mesut, and T. Aksoy, “Cryopreservation of blastocysts is the most feasible strategy in good responder patients,” *Fertility and Sterility*, vol. 96, no. 5, pp. 1121–1125.e1, 2011.
- [23] W. Yan, “An interview with Magdalena Zernicka-Goetz,” *Biology of Reproduction*, vol. 96, pp. 503–504, 2017.
- [24] A. Maheshwari, M. Hamilton, and S. Bhattacharya, “Should we be promoting embryo transfer at blastocyst stage,” *Reproductive BioMedicine Online*, vol. 32, no. 2, pp. 142–146, 2016.

Research Article

Identification of CeRNA Regulatory Networks in Atrial Fibrillation Using Nanodelivery

Ping Lin,¹ Lingqiang Meng,² and Lei Lyu ³

¹Department of Cardiology, Dongying Traditional Chinese Medicine Hospital, Dongying 257055, Shandong, China

²Department of Laboratory, Dongying Traditional Chinese Medicine Hospital, Dongying 257055, Shandong, China

³Department of Geriatrics, Dongying Traditional Chinese Medicine Hospital, Dongying 257055, Shandong, China

Correspondence should be addressed to Lei Lyu; lvlei@dyszyy.org.cn

Received 15 August 2022; Revised 5 September 2022; Accepted 9 September 2022; Published 29 September 2022

Academic Editor: Fernanda Tonelli

Copyright © 2022 Ping Lin et al. This is an open access article distributed under the Creative Commons Attribution License, which permits unrestricted use, distribution, and reproduction in any medium, provided the original work is properly cited.

The initiation and maintenance of AF is a complex biological process that is the ultimate manifestation of many cardiovascular diseases. And the pathogenesis of atrial fibrillation (AF) is unclear. Therefore, this study aimed to find the potential competing endogenous RNAs (ceRNAs) network and molecular dysregulation mechanism associated with AF. GSE135445, GSE2240, and GSE68475 were obtained from the Gene Expression Omnibus (GEO). Differential analysis was utilized to identify the differentially expressed mRNAs, miRNAs, and lncRNAs between AF and sinus rhythms (SR). AF-associated mRNAs and nanomaterials were screened and their biological functions and KEGG signaling pathways were identified. Nanomaterials for targeted delivery are uniquely capable of localizing the delivery of therapeutics and diagnostics to diseased tissues. The target mRNAs and target lncRNAs of differentially expressed miRNAs were identified using TargetScan and LncBase databases. Finally, we constructed the ceRNAs network and its potential molecular regulatory mechanism. We obtained 643 AF-associated mRNAs. They were significantly involved in focal adhesion and the PI3K-Akt signaling pathway. Among the 16 differentially expressed miRNAs identified, 31 differentially expressed target mRNAs, as well as 5 differentially expressed target lncRNAs were identified. Among them, we obtained 2 ceRNAs networks (hsa-miR-125a-5p and hsa-let-7a-3p). The aberrant expression of network target genes in AF mainly activated the HIF-1 signaling pathway. We speculated that the interaction pairs of miR-125a-5p and let-7a-3p with target mRNAs and target lncRNAs may be involved in AF. Our findings have a positive influence on investigating the pathogenesis of AF and identifying potential therapeutic targets.

1. Introduction

Atrial fibrillation (AF) is one of the most common arrhythmias and is strongly associated with poor quality of life, stroke, heart failure, and increased mortality [1]. AF has an incidence of up to 4% in modern Western populations and 0.5%–2% in Asian populations [2]. The lifetime risk for people aged 40 to 55 years has been estimated to be between 22% and 26% [3]. In 2010, the estimated number of people living with AF around the world was around 33.5 million [4]. Currently available treatments for AF have limited efficacy, and the mechanisms of development are poorly defined [5, 6]. Therefore, elucidating the exact molecular mechanisms of AF is urgently needed to identify suitable therapeutic targets. AF is one of the final manifestations of diverse

disease pathological processes, and its occurrence and maintenance cannot be explained by a single mechanism. Electrophysiological remodeling and structural remodeling have been reported to characterize the pathomechanism of AF [7]. Multiple molecular factors are involved in the progression of AF pathophysiology, including fibrosis, Ca²⁺ abnormalities, immune-inflammatory responses, and so on [8, 9].

Long noncoding RNAs (lncRNAs) are a class of transcripts greater than 200 NT in length that are involved in a variety of biological processes. Dysregulation of lncRNAs was found to be associated with many cardiac diseases, including AF [10]. MicroRNAs (miRNAs) are a class of small noncoding RNAs approximately 18–25 nucleotides in length that negatively regulate the expression of target genes by

binding to complementary sequences in 3'-untranslated regions (3'-UTRs) of target mRNAs, thereby promoting their degradation or inhibiting their translation [11]. Therefore, it is important to determine their role in the development of AF and whether they can be used to treat AF. It is well known that lncRNAs can play a certain role as a kind of competing endogenous RNA (ceRNA), thereby sequestering miRNAs away from target mRNAs [12]. These are also the ceRNA regulation guidelines. Bioinformatics analysis provided a new perspective to study the ceRNA involved in AF and laid a foundation for further investigation of their potential roles in AF. The enrichment results of differentially expressed mRNAs were the underlying molecular dysregulation mechanism of AF. Focal adhesion and extracellular matrix (ECM)-receptor interaction were reported to be associated with AF [13]. Focal adhesion group proteins are considered novel disease candidates with the potential to contribute to arrhythmia [14]. Abnormal deposition of ECM, which affects the maintenance of myocardial tissue structure, contributes to the pathological remodeling of AF [15]. There is evidence that downregulation of PI3K-Akt expression is associated with an increased incidence of AF in diabetic rats [16]. The PI3K-Akt pathway was confirmed to reduce the incidence of AF and attenuate atrial fibrosis [17].

Therefore, we aimed to screen differential genes in patients with AF, identify networks of AF-related molecular biological mechanisms, and explore key regulators during the progression of AF. In this study, the ceRNA network was established to facilitate the search for diagnostic and therapeutic targets associated with AF. In addition, enrichment analysis was performed on the differentially expressed mRNAs, and the signaling pathways regulated by the ceRNA network were identified. Several molecular mechanisms involved in cardiovascular remodeling are further highlighted. We believe that hsa-miR-125a-5p, hsa-let-7a-3p, and target genes may participate in the pathogenesis of AF through the HIF-1 signaling pathway.

2. Materials and Methods

2.1. Data Collection. GSE135445 included mRNA and lncRNA expression profiles of epicardial adipose samples from patients with persistent nonvalvular AF ($n=6$) and sinus rhythm (SR, $n=6$) based on the GPL20301 platform. GSE2240 included an mRNA expression profile of atrial tissue from 10 permanent AF and 20 SR based on the GPL97 platform. GSE68475 included miRNA expression profile of atrial right appendages from 10 samples were from patients with persistent AF and 11 normal SR based on the GPL15018 platform.

2.2. Difference Analysis. Difference analysis for mRNAs and lncRNAs between AF and SR in GSE135445 was performed using the edger R package [18]. The limma R package [19] was used for the difference analysis of mRNAs and miRNAs between AF and SR in GSE2240 and GSE68475. P value <0.05 was used to define significant differentially expressed mRNAs (DEmRs), differentially expressed

lncRNAs (DELncRs), and differentially expressed miRNAs (DEmiRs) in the results of the difference analysis.

2.3. Functional and Pathway Enrichment. The enrichment analysis of Gene Ontology (GO) and Kyoto Encyclopedia of Genes and Genomes (KEGG) pathway enrichment analysis for mRNAs was performed using the clusterProfiler R package [20]. The biological process (BP) was one kind of GO enrichment. The $P < 0.05$ was set as the threshold of statistical significance. Gene set variation analysis (GSVA) was performed using the GSVA R package to display enrichment results of target mRNAs. To identify the underlying molecular dysregulation mechanisms of AF, we performed an enrichment analysis of AF-associated mRNAs. These mRNAs were enriched to three ontologies of GO: cellular component (CC), molecular function (MF), and biological process (BP).

2.4. Immune Cell Infiltration. The xCell R package [21] was used to assign and visualize 31 types of immune cells in AF and SR samples based on ssGSEA (single-sample gene set enrichment analysis) in GSVA (gene set variation analysis). P value <0.05 was considered statistically significant for xCell scores between AF and SR which were calculated with the limma R package.

2.5. Target Prediction and CeRNA Network Construction. The LncBase Predicted v.2 was used to predict the target lncRNAs regulated by differentially expressed miRNAs. The screening threshold was set as 0.7. Then, the target mRNAs regulated by differentially expressed miRNAs were predicted using TargetScan (https://www.targetscan.org/vert_72/) database. The ceRNA network was established from the differentially expressed lncRNAs, miRNAs, and mRNAs. CeRNA networks identified by us included a downregulated lncRNA (AC125807.2) that was regulated by upregulated hsa-miR-125a-5p, as well as downregulated mRNAs (EGFR, MACF1, TRPS1, EEF1A1, MASP1, PANX1, PUM2, CGNL1, NPM1, and TFRC). Upregulated lncRNA (LINC01139) and upregulated mRNA (SRI) were regulated by downregulated hsa-let-7a-3p.

3. Results

3.1. Identification of AF-Associated mRNAs. To identify AF-associated mRNAs, we performed differential expression analysis of mRNAs in GSE135445. By threshold screening, we obtained 1556 differentially expressed mRNAs between AF and SR (Figure 1(a)). These included 733 upregulated differentially expressed and 823 downregulated differentially expressed (Figure 1(b)). We obtained 7084 differentially expressed mRNAs in GSE2240, and by comparing them with those of GSE135445, we identified 643 common differentially expressed mRNAs (Figure 1(c)). There were significant differences in the expression of common mRNAs between AF and SR samples in GSE2240 (Figure 1(d)), and they may be AF-associated mRNAs.

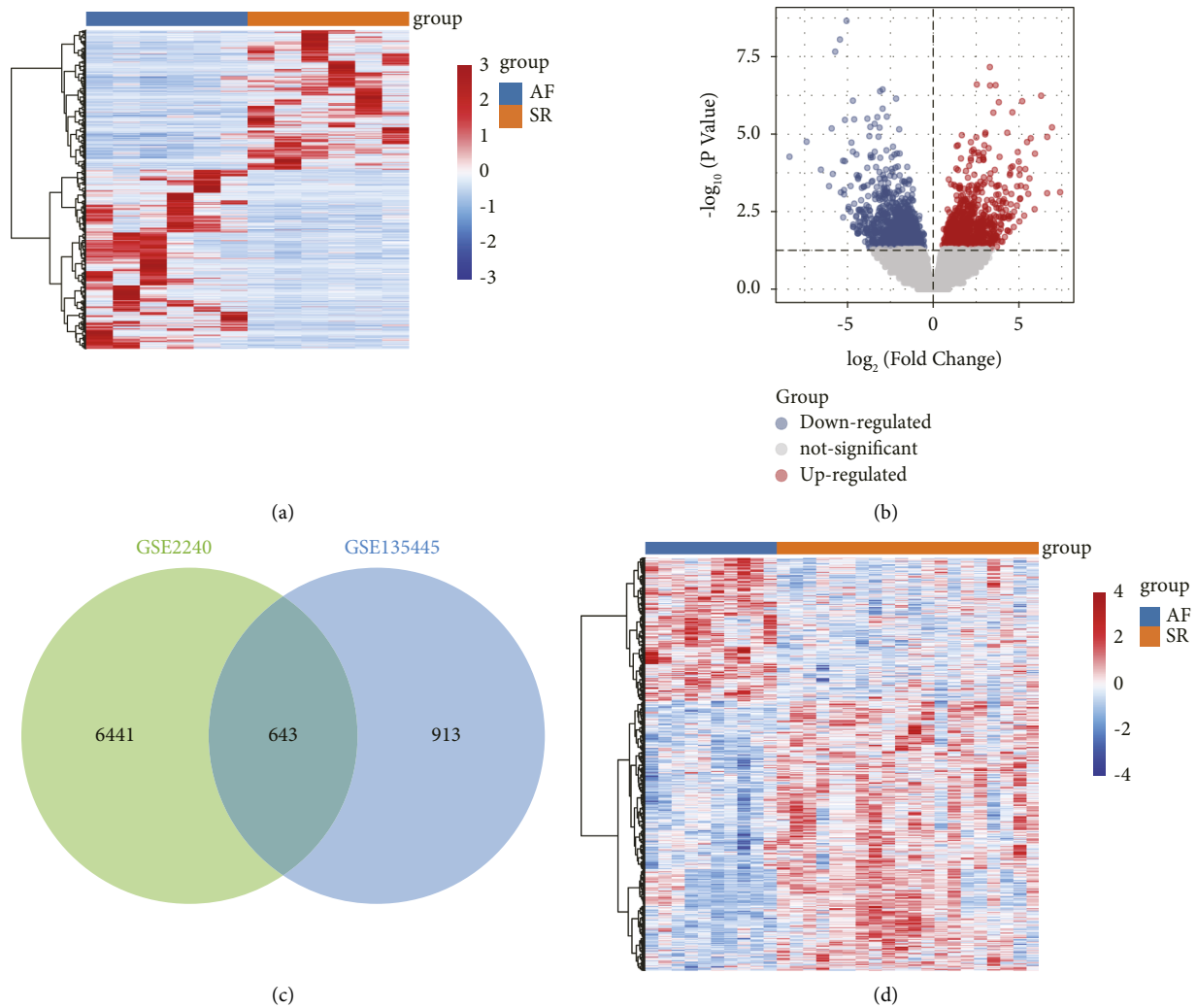


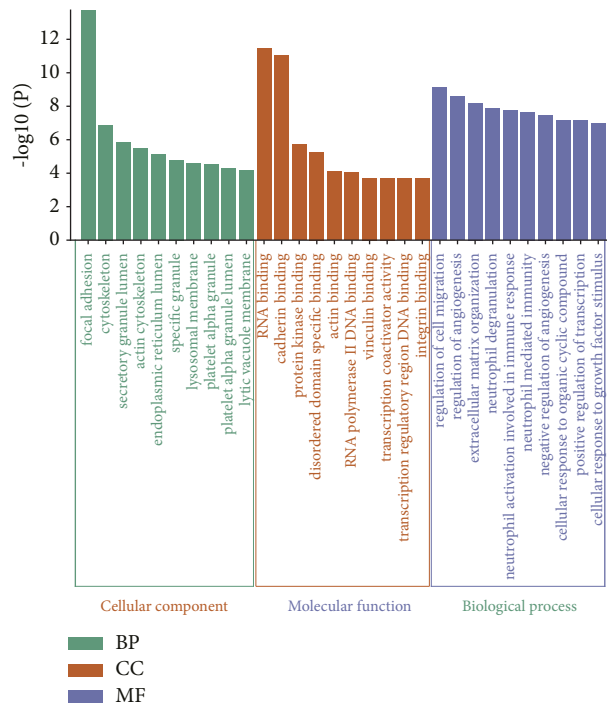
FIGURE 1: Screening of differentially expressed mRNAs between AF and SR. (a). Heatmap of differentially expressed mRNAs between AF and SR in GSE135445. (b). Volcano plot of differentially expressed mRNAs between AF and SR in GSE135445. Red is upregulated and blue is downregulated. (c). Venn diagram of differentially expressed mRNAs in GSE135445 and GSE2240. (d). Heatmap of common mRNAs in GSE2240.

3.2. Biological Functions of Common mRNAs. Figure 2(a) shows the top 10 GO terms in AF-associated mRNAs enrichment. In CC results, we identified significantly enriched focal adhesion, cytoskeleton, and secretory granule lumen. RNA binding, cadherin binding, and protein kinase binding were significantly enriched in MF. And regulation of cell migration, regulation of angiogenesis, and neutrophil-mediated immunity were significantly enriched in BP. In addition, we found focal adhesion, PI3K-Akt signaling pathway, and ECM-receptor interaction to be significantly enriched in KEGG results (Figure 2(b)). On the other hand, we calculated the infiltration of immune cells in AF patients. CD8+ naïve T cell and Th1 cell infiltration were significantly higher in AF, whereas macrophage M1 and Th2 cell infiltration were significantly lower in AF, compared with SR (Figure 2(c)).

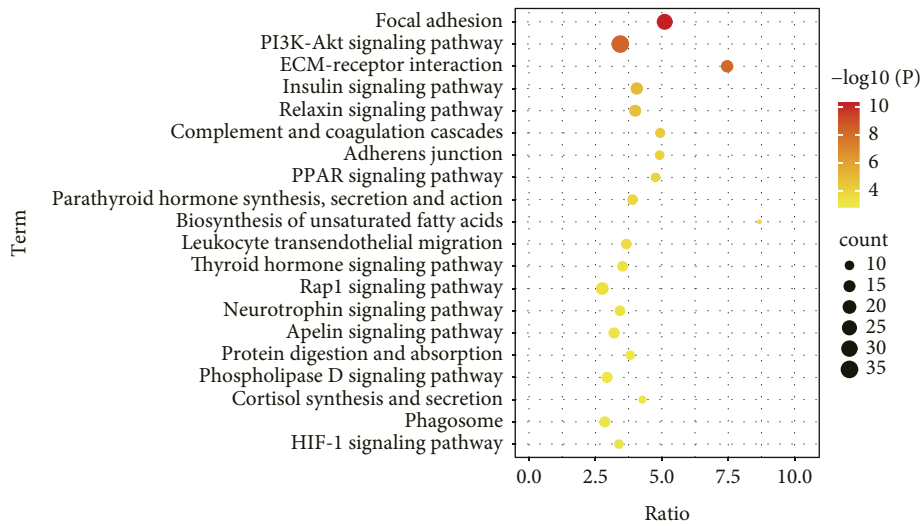
3.3. Differentially Expressed miRNAs and lncRNAs. Sixteen differentially expressed miRNAs in GSE68475 were identified in AF patients after comparison with Sr

(Figure 3(a)). In GSE135445, we found 286 differentially expressed lncRNAs between AF and SR (Figure 3(b)). Using the TargetScan database, we identified 529 target mRNAs of the differentially expressed miRNAs. Comparing with the differentially expressed mRNAs, we obtained 31 differentially expressed target mRNAs (Figure 3(c)). Using the LncBase database, we identified 2358 target lncRNAs of differentially expressed miRNAs. Compared with the differentially expressed lncRNAs, we obtained 5 differentially expressed target lncRNAs (Figure 3(c)).

3.4. CeRNA (DElncRs-DEmiRs-DEmRs) Regulatory Network. According to the ceRNA regulation guidelines, the two ceRNA networks were established by Cytoscape software (Figure 4(a)), which included upregulated hsa-miR-125a-5p, downregulated lncRNAs, and mRNAs target, as well as downregulated hsa-let-7a-3p, upregulated lncRNAs, and mRNAs target. The results of enrichment analysis showed that the target mRNAs were mainly involved in the HIF-1



(a)



(b)

FIGURE 2: Continued.

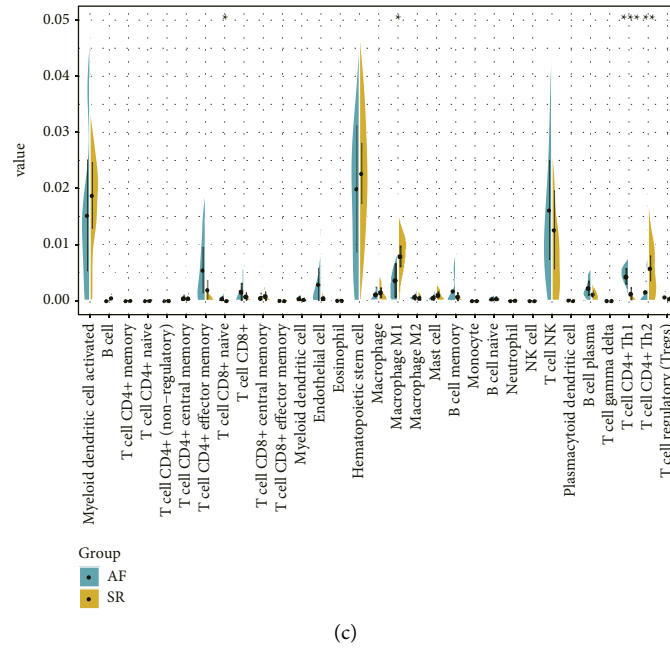


FIGURE 2: Identification of potential molecular maladjustment mechanisms of AF. (a). The top 10 GO terms in AF associated mRNAs enrichment. (b). Significantly enriched KEGG pathways of AF-associated mRNAs. (c). Levels of immune cell infiltration in patients with AF and SR. * $P < 0.05$, ** $P < 0.01$, *** $P < 0.001$.

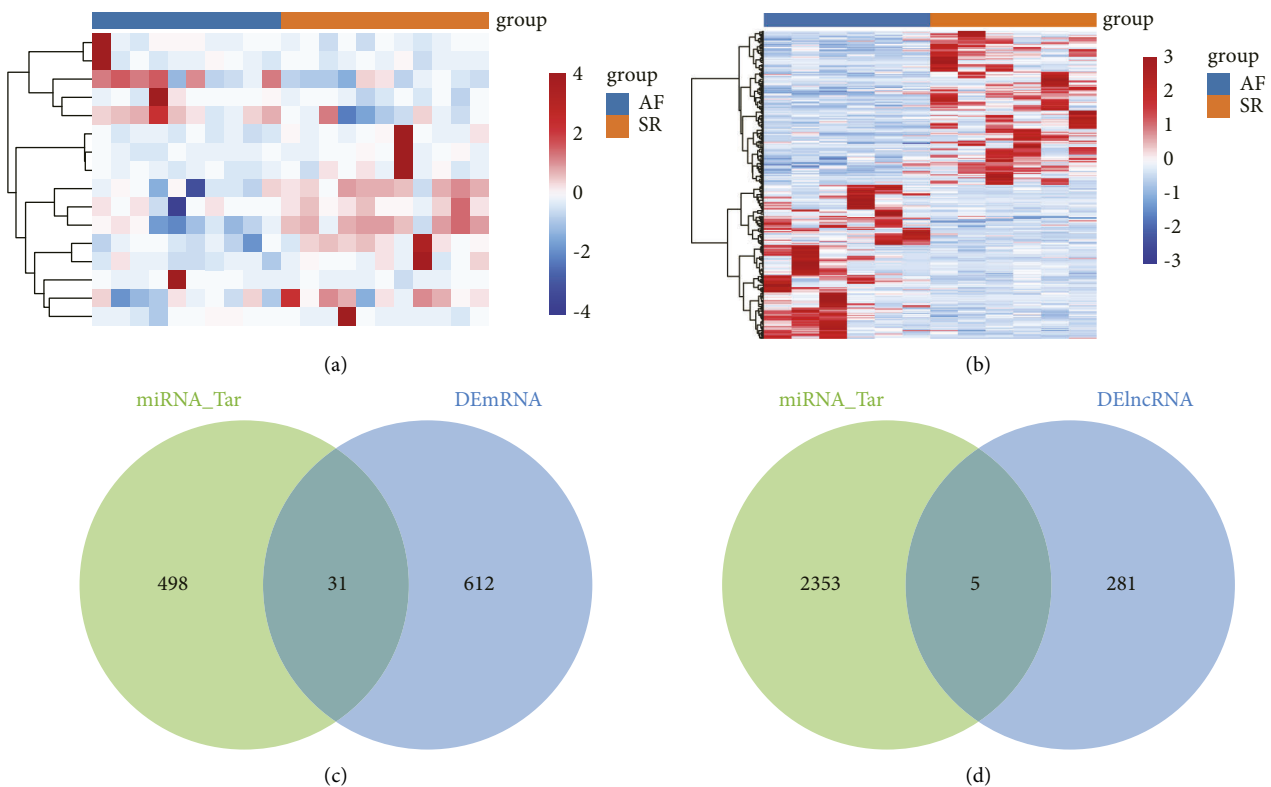
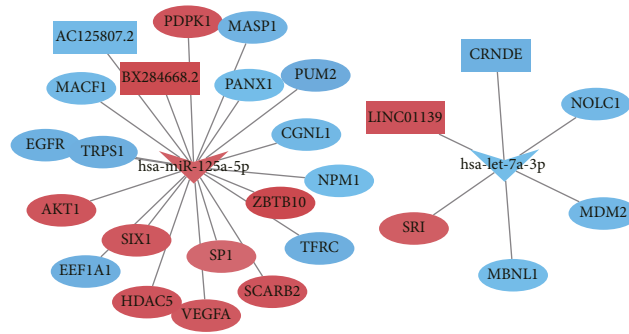
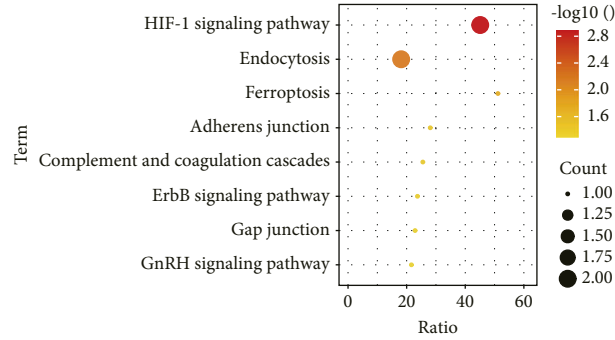


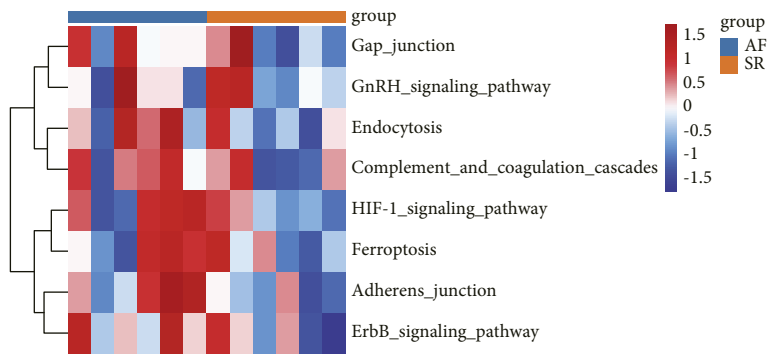
FIGURE 3: Identification of differentially expressed miRNAs and prediction of their target lncRNAs and mRNAs. (a). The differentially expressed miRNAs between AF and SR in GSE68475. (b). The differentially expressed lncRNAs between AF and SR in GSE135445. (c). The intersection of target mRNAs and differentially expressed mRNAs. (d). The intersection of target lncRNAs and differentially expressed lncRNAs.



(a)



(b)



(c)

FIGURE 4: Continued.

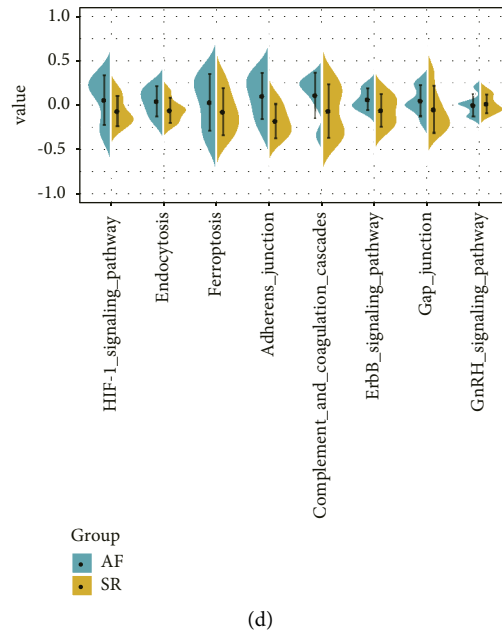


FIGURE 4: The lncRNA-miRNA-mRNA network in AF. (a). The ceRNA network in AF. Rectangles, triangles, and circles represent lncRNAs, miRNAs, and mRNAs, respectively. (b). Significant KEGG signaling pathways are involved in the target genes. (c). Heatmap of the score of signaling pathways calculated GSEA in AF and SR. (d). Differential analysis identified signaling pathways activated or inhibited in AF compared with SR.

signaling pathway, endocytosis, and ferroptosis (Figure 4(b)). Using GSEA, we evaluated the expression of these signaling pathways in AF patients (Figure 4(c)). Comparison with SR found that the GnRH signaling pathway was inhibited in AF and the other signaling pathways were all activated in AF (Figure 4(d)):

4. Discussion

In recent years, with the rapid development of high-throughput technologies, researchers have been able to observe changes in molecular regulatory mechanisms at the gene expression level. In this study, we used transcriptome data of AF patients from public databases containing mRNAs, lncRNAs, and miRNAs. A total of 643 differentially expressed mRNAs, 286 differentially expressed lncRNAs, and 16 differentially expressed miRNAs were identified. In the results of enrichment analysis, the differentially expressed mRNAs were mainly associated with focal adhesion, PI3K-Akt signaling pathway, and ECM-receptor interaction. In addition, we identified a significant infiltration level of immune cells in AF. Importantly, we successfully constructed a ceRNA network to further understand the underlying regulatory mechanism of AF.

Interestingly, we identified 2 ceRNA networks. Consistent with the results of our analysis, miR-125a-5p was upregulated in patients with AF [22]. Studies have shown that genetic polymorphisms of miR-125a are associated with the recurrence of AF [23]. Moreover, dysregulated miR-125a-5p expression is associated with the formation of vascular plaques and vascular restenosis [24]. In addition, hsa-let-7a-3p expression was downregulated in AF

compared with SR [25]. Khudiakov et al. showed that hsa-let-7a-3p was abnormally expressed in cardiovascular disease [26]. It is shown that let-7a-3p acts as a tumor suppressor and participates in the regulatory processes of proliferation and apoptosis in cancer cells [27].

Here, the results of our analysis suggest that AC125807.2 is a regulator of AF and competitively binds to miR-125a-5p with multiple target mRNAs. Among them, p38-mitogen-activated protein kinase has been implicated in AF and atrial remodeling after epidermal growth factor receptor (EGFR) activation [28]. EGFR is required for cardiovascular function and its deletion produces cardiac damaging effects [29]. MACF1 has a regulatory effect on the focal adhesion of the cytoskeleton [30]. In addition, LINC01139 is competitively bound to let-7a-3p with SRI, thereby participating in the molecular regulation of AF. Sorcin (SRI), an accessory binding protein, regulates sarcoplasmic reticulum Ca²⁺ release and has important functions in the pathogenesis of AF [31, 32]. Seidler et al. showed that SRI overexpression affects cardiomyocyte excitation-contraction coupling [33].

Among the signaling pathways regulated by the ceRNA network, we found that the HIF-1 signaling pathway was significantly activated in AF. Hypoxia-inducible factor-1 (HIF-1) is a regulator that regulates the body's response to hypoxia-induced angiogenesis [34]. Atrial hypoxia promotes atrial fibrillation substrate formation by promoting atrial structural remodeling [35]. In the early response of cardiomyocytes to AF, the expression of genes of HIF-1 α was increased in synchrony with the onset of atrial myofibroblasts [36]. Activation of the gonadotropin-releasing hormone (GnRH) receptor is associated with coronary heart disease and myocardial infarction [37]. However, in

the results of our analysis, the GnRH signaling pathway was significantly inhibited. This is consistent with the findings of Chiang et al. [38]. These results suggest that the ceRNA network may be involved in the development of AF through the regulatory mechanisms of HIF-1 and GnRH signaling during the pathogenesis of AF, but these mechanisms require further investigation.

5. Conclusion

We identified two ceRNA networks, including hsa-miR-125a-5p, hsa-let-7a-3p, and target genes. They may participate in the pathogenesis of AF through the HIF-1 signaling pathway. These results provide a partial description of the comprehensive regulatory network of AF, which may help provide new insights into the pathogenesis of AF and identify potential therapeutic targets. However, there are also certain limitations in this study. First, considering our low number of analyzed samples, more samples are needed. Second, we provided two sets of AF-related ceRNA networks, but further experimental validation is needed. We hope to conduct further studies in large-scale clinical samples to identify potential regulatory mechanistic memory therapeutic targets.

Data Availability

The datasets used and/or analyzed during the current study are available from the corresponding author upon reasonable request.

Conflicts of Interest

The author(s) declares no potential conflicts of interest with the respect to the research, authorship, and/or publication of this article.

References

- [1] X. Hu, L. Chen, S. Wu et al., "Integrative analysis reveals key circular RNA in atrial fibrillation," *Frontiers in Genetics*, vol. 10, p. 108, 2019.
- [2] M. Kraft, A. Buscher, F. Wiedmann et al., "Current drug treatment strategies for atrial fibrillation and TASK-1 inhibition as an emerging novel therapy option," *Frontiers in Pharmacology*, vol. 12, Article ID 638445, 2021.
- [3] J. Pellman and F. Sheikh, "Atrial fibrillation: mechanisms, therapeutics, and future directions," *Comprehensive Physiology*, vol. 5, no. 2, pp. 649–665, 2015.
- [4] S. S. Chugh, R. Havmoeller, K. Narayanan et al., "Worldwide epidemiology of atrial fibrillation: a global burden of disease 2010 study," *Circulation*, vol. 129, no. 8, pp. 837–847, 2014.
- [5] F. Cao, Z. Li, W. M. Ding, L. Yan, and Q. Y. Zhao, "LncRNA PVT1 regulates atrial fibrosis via miR-128-3p-Sp1-TGF- β 1-Smad axis in atrial fibrillation," *Molecular Medicine*, vol. 25, no. 1, p. 7, 2019.
- [6] T. Liu, G. Zhang, Y. Wang et al., "Identification of circular RNA-microRNA-messenger RNA regulatory network in atrial fibrillation by integrated analysis," *BioMed Research International*, vol. 2020, Article ID 8037273, 13 pages, 2020.
- [7] W. Li, L. Wang, Y. Wu, Z. Yuan, and J. Zhou, "Weighted gene coexpression network analysis to identify key modules and hub genes associated with atrial fibrillation," *International Journal of Molecular Medicine*, vol. 45, no. 2, pp. 401–416, 2020.
- [8] S. Nattel, "Molecular and cellular mechanisms of atrial fibrosis in atrial fibrillation," *Journal of the American College of Cardiology: Clinical Electrophysiology*, vol. 3, no. 5, pp. 425–435, 2017.
- [9] R. Ferrari, M. Bertini, C. Blomstrom-Lundqvist et al., "An update on atrial fibrillation in 2014: from pathophysiology to treatment," *International Journal of Cardiology*, vol. 203, pp. 22–29, 2016.
- [10] J. Du, Z. Li, X. Wang et al., "Long noncoding RNA TCONS-00106987 promotes atrial electrical remodeling during atrial fibrillation by sponging miR-26 to regulate KCNJ2," *Journal of Cellular and Molecular Medicine*, vol. 24, no. 21, Article ID 12788, 2020.
- [11] T. A. Farazi, J. I. Hoell, P. Morozov, and T. Tuschl, "MicroRNAs in human cancer," *Advances in Experimental Medicine and Biology*, vol. 774, pp. 1–20, 2013.
- [12] U. Ala, "Competing endogenous RNAs, non-coding RNAs and diseases: an intertwined story," *Cells*, vol. 9, no. 7, p. 1574, 2020.
- [13] Y. Oh, S. Yang, X. Liu et al., "Transcriptomic bioinformatic analyses of atria uncover involvement of pathways related to strain and post-translational modification of collagen in increased atrial fibrillation vulnerability in intensely exercised mice," *Frontiers in Physiology*, vol. 11, Article ID 605671, 2020.
- [14] C. J. Nalliah, J. R. Bell, A. J. A. Raaijmakers et al., "Epicardial adipose tissue accumulation confers atrial conduction abnormality," *Journal of the American College of Cardiology*, vol. 76, no. 10, pp. 1197–1211, 2020.
- [15] E. R. Lubbers, M. V. Price, and P. J. Mohler, "Arrhythmogenic substrates for atrial fibrillation in obesity," *Frontiers in Physiology*, vol. 9, p. 1482, 2018.
- [16] F. L. Zhang, S. L. Chu, W. W. Wang, and L. L. Chen, "Downregulated PI3K-Akt-eNOS expression is related to increased atrial fibrillation inducibility in diabetic rats," *Zhonghua Xinxueguanbing Zazhi*, vol. 46, no. 5, pp. 376–381, 2018.
- [17] D. N. Misra, H. W. Kunz, A. Kanbour, and T. J. Gill 3rd, "Characterization of the pregnancy-associated rat MHC class I antigen Pa by mating studies and by peptide mapping," *Transplantation Proceedings*, vol. 21, no. 1, pp. 561–562, 1989.
- [18] M. D. Robinson, D. J. McCarthy, and G. K. Smyth, "edgeR: a bioconductor package for differential expression analysis of digital gene expression data," *Bioinformatics*, vol. 26, no. 1, pp. 139–140, 2010.
- [19] M. E. Ritchie, B. Phipson, D. Wu et al., "Limma powers differential expression analyses for RNA-sequencing and microarray studies," *Nucleic Acids Research*, vol. 43, no. 7, p. e47, 2015.
- [20] G. Yu, L. G. Wang, Y. Han, and Q. Y. He, "ClusterProfiler: an R package for comparing biological themes among gene clusters," *OMICS: A Journal of Integrative Biology*, vol. 16, no. 5, pp. 284–287, 2012.
- [21] D. Aran, Z. Hu, and A. J. Butte, "xCell: digitally portraying the tissue cellular heterogeneity landscape," *Genome Biology*, vol. 18, no. 1, p. 220, 2017.
- [22] A. M. G. D. Silva, J. N. G. D. Araújo, R. C. C. D. Freitas, and V. N. Silbiger, "Circulating MicroRNAs as potential biomarkers of atrial fibrillation," *BioMed Research International*, vol. 2017, Article ID 7804763, 7 pages, 2017.
- [23] X. B. Shen, S. H. Zhang, H. Y. Li et al., "Rs12976445 polymorphism is associated with post-ablation recurrence of atrial

- fibrillation by modulating the expression of MicroRNA-125a and interleukin-6R,” *Medical Science Monitor*, vol. 24, pp. 6349–6358, 2018.
- [24] H. A. Cakmak and M. Demir, “MicroRNA and cardiovascular diseases,” *Balkan Medical Journal*, vol. 37, no. 2, pp. 60–71, 2020.
- [25] H. Liu, H. Qin, G. X. Chen et al., “Comparative expression profiles of microRNA in left and right atrial appendages from patients with rheumatic mitral valve disease exhibiting sinus rhythm or atrial fibrillation,” *Journal of Translational Medicine*, vol. 12, no. 1, p. 90, 2014.
- [26] A. A. Khudiakov, D. D. Panshin, Y. V. Fomicheva et al., “Different expressions of pericardial fluid microRNAs in patients with arrhythmogenic right ventricular cardiomyopathy and ischemic heart disease undergoing ventricular tachycardia ablation,” *Frontiers in Cardiovascular Medicine*, vol. 8, Article ID 647812, 2021.
- [27] Z. Dong, Q. Lei, R. Yang et al., “Inhibition of neurotensin receptor 1 induces intrinsic apoptosis via let-7a-3p/Bcl-w axis in glioblastoma,” *British Journal of Cancer*, vol. 116, no. 12, pp. 1572–1584, 2017.
- [28] R. Coppini, L. Santini, C. Palandri, L. Sartiani, E. Cerbai, and L. Raimondi, “Pharmacological inhibition of serine proteases to reduce cardiac inflammation and fibrosis in atrial fibrillation,” *Frontiers in Pharmacology*, vol. 10, p. 1420, 2019.
- [29] B. Schreier, S. Rabe, S. Winter et al., “Moderate inappropriately high aldosterone/NaCl constellation in mice: cardiovascular effects and the role of cardiovascular epidermal growth factor receptor,” *Scientific Reports*, vol. 4, no. 1, p. 7430, 2014.
- [30] E. Forkosh, A. Kenig, and Y. Ilan, “Introducing variability in targeting the microtubules: review of current mechanisms and future directions in colchicine therapy,” *Pharmacology Research & Perspectives*, vol. 8, no. 4, Article ID e00616, 2020.
- [31] D. Dobrev and X. H. Wehrens, “Calmodulin kinase II, sarcoplasmic reticulum Ca²⁺ leak, and atrial fibrillation,” *Trends in Cardiovascular Medicine*, vol. 20, no. 1, pp. 30–34, 2010.
- [32] G. Santulli, G. Iaccarino, N. De Luca, B. Trimarco, and G. Condorelli, “Atrial fibrillation and microRNAs,” *Frontiers in Physiology*, vol. 5, p. 15, 2014.
- [33] T. Seidler, S. L. Miller, C. M. Loughrey et al., “Effects of adenovirus-mediated sorcin overexpression on excitation-contraction coupling in isolated rabbit cardiomyocytes,” *Circulation Research*, vol. 93, no. 2, pp. 132–139, 2003.
- [34] M. Hong, H. Shi, N. Wang, H. Y. Tan, Q. Wang, and Y. Feng, “Dual effects of Chinese herbal medicines on angiogenesis in cancer and ischemic stroke treatments: role of HIF-1 network,” *Frontiers in Pharmacology*, vol. 10, p. 696, 2019.
- [35] C. F. Tsai, S. F. Yang, C. H. Lo, H. J. Chu, and K. C. Ueng, “Role of the ROS-JNK signaling pathway in hypoxia-induced atrial fibrotic responses in HL-1 cardiomyocytes,” *International Journal of Molecular Sciences*, vol. 22, no. 6, p. 3249, 2021.
- [36] V. L. Thijssen, H. M. van der Velden, E. P. van Ankeren et al., “Analysis of altered gene expression during sustained atrial fibrillation in the goat,” *Cardiovascular Research*, vol. 54, no. 2, pp. 427–437, 2002.
- [37] C. S. Saigal, J. L. Gore, T. L. Krupski et al., “Androgen deprivation therapy increases cardiovascular morbidity in men with prostate cancer,” *Cancer*, vol. 110, no. 7, pp. 1493–1500, 2007.
- [38] D. Y. Chiang, M. Zhang, N. Voigt et al., “Identification of microRNA-mRNA dysregulations in paroxysmal atrial fibrillation,” *International Journal of Cardiology*, vol. 184, pp. 190–197, 2015.